Geological Survey of Finland

2022

Indications of flake graphite and Ni–Co–Au mineralization in metavolcanic sequences in Emas, Kruunupyy, western Finland

Janne Kuusela, Henrik Nygård, Dandara Salvador, Thair Al-Ani, Jukka-Pekka Kujasalo, Hanna Leväniemi, Noora Thurman, Helena Hulkki, Anne Taivalkoski, Teo Lehto and Jukka Kuva

GTK Open File Research Report 44/2022

GTK

GEOLOGICAL SURVEY OF FINLAND

Open File Research Report 44/2022

Janne Kuusela, Henrik Nygård, Dandara Salvador, Thair Al-Ani, Jukka-Pekka Kujasalo, Hanna Leväniemi, Noora Thurman, Helena Hulkki, Anne Taivalkoski, Teo Lehto and Jukka Kuva

Indications of flake graphite and Ni–Co–Au mineralization in metavolcanic sequences in Emas, Kruunupyy, western Finland

Unless otherwise indicated, the figures have been prepared by the authors of the report.

Front cover: The metavolcanic rocks in the Aho and Raisjoki belts in western Finland have high battery mineral potential. Photo: Janne Kuusela, GTK.

Layout: Elvi Turtiainen Oy

Espoo 2022

Kuusela, J., Nygård, H., Salvador, D., Al-Ani, T., Kujasalo, J.-P., Leväniemi, H., Thurman, N., Hulkki, H., Taivalkoski, A., Lehto, T. & Kuva, J. 2022. Indications of flake graphite and Ni–Co–Au mineralization in metavolcanic sequences in Emas, Kruunupyy, western Finland. *Geological Survey of Finland, Open File Research Report 44/2022*, 43 pages, 37 figures, 7 tables and 3 appendices.

GTK discovered a new flake graphite occurrence with an additional low-grade Ni–Co–Au mineralization in the Aho belt, a metavolcanic rock sequence located in Emas, Kruunupyy, western Finland. The results of drilling assays verified a flake graphite content of >7% in several black schist sections of up to 15 m in length, and in neighbouring parallel layered volcanic rocks, Ni–Co–Au reached grades as high as 3 m @ 0.5% Co and 2% Ni, with a 2-m section of 0.34 ppm Au or 10.5 m of 0.11% Co and 0.8% Ni. The main ore-forming minerals containing Ni–Co–Au were identified as, gersdorffite, Co – arsenopyrite, cobaltite and pentlandite. A significant rise in Ni–Co concentrations in sections of 15 m or greater could be followed to the north and south, with an average Co content of 100–200 ppm and a Ni content varying from 0.1–0.2%. Each Ni–Co section with anomalous Ni and Co was enveloped by high Cr values, suggesting an ultramafic contribution to the mineralization. Besides flake graphite, the black schists also contained Zn in sphalerite and anomalous U present as uraninite. The U content appears to closely reflect the graphite and zinc content, especially if the rock contains more than 4% Cg. A mineralogical overview confirmed flake graphite sections in every drill hole in the Emas black schist, with a flake size ranging from 30 to 200 µm, and samples were therefore sent for bench-scale tests to GTK Mintec in Outkumpu. The tests involved crushing, grinding, flotation and purification by alkaline roasting and acid leaching. Using ultrafine grinding before three flotation stages proved most efficient, giving a concentrate of 89% purity and 66.2% recovery. After the purification process, a Cg grade of >99% was achieved.

The Emas study area is one of six targets studied in the so-called Raisjoki investigation area, covering 900 km2 in the municipalities of Krunupyy, Evijärvi and Veteli. The new discoveries were sighted in 2019 at the beginning of a four-year battery mineral project (2019–2022). Before two small drilling campaigns with a total of 9 drill holes, the area was probed by geophysical measurements, including magnetic, multi-frequency electromagnetic (EM) and gravity measurements. Magnetic and EM measurements were continued towards the N and S after the drilling campaigns.

The continuation of the sulphide mineralization in the N and S was traced by 144 surface moraine samples. Indicators of a possible continuation could be traced along the continuation of the volcanic sequence one kilometre further south. A sudden large contrast in Ca/Cr values in assay results from the moraine samples suggests possible fault or shear zones cutting the volcanic sequences.

The Emas flake graphite is found in an area with an exceptionally low metamorphic signature. The investigations indicate that the black schists in the volcanic sequences commonly associated with spodumene pegmatites contain a good potential for flake graphite, a potential that may be applied to the whole region. Structures visible through geophysical signals such as gravity signals and surficial Cr anomalies within or in close proximity to black shists could also serve as pathfinders for Ni–Co–Au mineralizations.

Keywords: graphite, beneficiation, metavolcanic rock, cobalt, nickel, battery minerals, Emas, Kruunuypyy, Ostrobothnia, Western Finland

Janne Kuusela
Geological Survey of Finland
P.O. Box 96
FI-02151 Espoo, Finland

E-mail: janne.kuusela@gtk.fi

Kuusela, J., Nygård, H., Salvador, D., Al-Ani, T., Kujasalo, J.-P., Leväniemi, H., Thurman, N., Hulkki, H., Taivalkoski, A., Lehto, T. & Kuva, J. 2022. Indications of flake graphite and Ni–Co–Au mineralization in metavolcanic sequences in Emas, Kruunupyy, western Finland. Tiivistelmä: Indikaatioita suomugrafiitti sekä Ni–Co–Au mineralisaatioista metavulkaanisessa jaksossa Kruunupyyn Emaksessa. *Geologian tutkimuskeskus, Tutkimustyöraportti 44/2022*, 43 sivua, 37 kuvaa, 7 taulukkoa ja 3 liitettä.

GTK löysi uuden suomugrafiittiesiintymän Ahon vulkaniittijaksolla vuosina 2019–2022 toteutetun akkumineraaliprojektin yhteydessä Kruunupyyn Emas-kohteessa, Pohjanmaalla. Kairauksissa lävistettiin useampia keskimääräisesti yli 7 % grafiittia (Cg) sisältäviä jopa 15 m paksuja mustaliuskeosueita, joiden mineralogisissa alkuselvityksissä todettiin sisältävän 30–200 µm:n kokoista suomugrafiittia. Suomugrafiittiaiheen rinnakkaisena mineralisaationa löytyi myös osittain semimassiivinen Ni–Co–Au-aihe, jonka paras lävistys oli 3 m 0,5 % Co ja 2 % Ni, jossa 2 m 0,34 ppm Au tai vaihtoehtoisesti 10,5 m 0,11 % Co ja 0,8 % Ni. Päämineraaleina sulfidimineralisaatiossa olivat gersdorfiitti, cobaltiitti, Co-arseenikiisu sekä pentlandiitti. Ni–Co-vyöhyke jatkuu sekä pohjoiseen että etelään päälävistyksestä ja on lävistetty useammassa kairareiässä noin 15 m + matkalla, jossa Co keskimääräiset pitoisuudet ovat 100–200 ppm ja Ni 0,1–0,2 %:n pitoisuuksilla. Tyypillisesti kohonneisiin Ni–Co-pitoisuuksiin liittyy myös selvästi kohonneita Cr-pitoisuuksia, jotka viittaavat mahdolliseen ultramaafiseen vaikutukseen mineralisaation synnyssä. Mustaliuskeet sisältävät myös kohonneita Zn-pitoisuuksia, joka esiintyy sinkkivälkkeenä, sekä kohonneita U-pitoisuuksia, joka esiintyy kivissä uraniniittina. Uraanipitoisuus korreloi hyvin grafiitti- sekä sinkkipitoisuuden kanssa varsinkin, jos grafiittipitoisuus (Cg) > 4 %. Lupaavien mineralogisten laatuselvitysten jälkeen Emaksen grafiittipitoisia kivinäytteitä lähetettiin GTK Mintec Outokumpuun rikastuskokeisiin. Rikastusprosessi sisälsi murskauksen, jauhatuksen, vaahdotuksen sekä rikasteen puhdistamisen pasutuksella ja happoliuotuksella. Ultrahienolla jauhatuksella ennen kolmea vaahdotusvaihetta saatiin (Cg) 89 %:n puhtausasteen omaava rikaste 66,2 %:n saannilla. Pasutuksen ja liuotuksen jälkeen rikasteen puhtausaste ylitti 99 %.

Emaksen tutkimuskohde on yksi kuudesta kohteesta ”Raisjoki”-nimen saaneelle tutkimusalueelle, joka kattaa 900 km2 ja sijoittuu pääosin Kruunupyyn, Evijärven ja Vetelin alueille. Ennen timanttikairauksia (yht. yhdeksän reikää) suoritettiin geofysikaalisia mittauksia, jotka sisälsivät magneettisia, painovoima- sekä kallioperän johtavuusmittauksia ja joita jatkettiin myös kairauksien jälkeen.

Mineralisaation jatkeita sekä pohjoiseen että etelään selvitettiin pintamoreeninäytteenotolla, jossa otettiin yhteensä 144 näytettä. Viitteitä mineralisaation jatkeista on havaittavissa ainakin vulkaniittijakson jatkeessa n. 1 km:n päässä mineralisaation eteläsuunnassa. Pintamoreenituloksissa havaitut äkkinäiset heitot Ca–Cr-suhteessa viittaavat vulkaniittijaksoa leikkaaviin siirrostumiin ym. rakenteisiin vulkaniittijaksossa.

Emaksen suomugrafiittiesiintymä löytyi alueella, jossa on esiintymälle epätyypillisen alhainen metamorfoosiaste. Tutkimukset osoittavat, että mustaliuskeita sisältävät vulkaniittivyöhykkeet, joita varsinkin Keski-Pohjanmaan alueella voidaan yhdistää spodumeenipegmatiitteihin, omaavat suuren suomugrafiittipotentiaalin. Tämän lisäksi vulkaniittivyöhykkeiden geofysikaaliset rakenne ja painovoimaviitteet yhdistettynä pintamoreeninäytteenoton Cr-anomalioihin voivat toimia hyvinä viitteinä myös uusille Ni–Co–Au-aiheille.

Asiasanat: grafiitti, rikastus, metavulkaaninen kivi, koboltti, nikkeli, akkumineraalit, Emas, Kruunupyy, Pohjanmaa, Länsi-Suomi

Janne Kuusela
Geologian tutkimuskeskus
PL 96
02151 Espoo

Sähköposti: janne.kuusela@gtk.fi

CONTENTS

1 INTRODUCTION

In 2020, the EU published the fourth list of critical raw materials (CRM) in a communication on critical raw materials. As conventional grade resources are becoming depleted new lower-grade alternatives should be overviewed and investigated to secure future needs.

Besides natural graphite, black schists are also known to contain low grades of base metals, some of which are listed as critical minerals (CRM) in the EU. The Sotkamo black schists are already being extracted from raw materials suitable for the battery industry from a low-grade ore resource. Black schists are abundant in the Finnish bedrock, but quality assessment of black schist graphite to determine its suitability for batteries has so far been limited.

The metavolcanic belts cutting the Ostrobothnian schist belt in western Finland have been sites for exploration due to the discovery of associated spodumene pegmatites, mainly in the Kaustinen region (Säynäjärvi 1973, Kuusela et al. 2011). The metavolcanic rocks contain abundant layers of graphite-rich schists that also contain low grades of sulphides.

The sulphide-rich boulders revealed in the Raisjoki belt in the east of the Aho formation became a popular site for layman sampling in the 1960s. Some of the samples have displayed an exceptionally high content of Cu, Ni and Co, which led to the execution of several geophysical and geological investigation programmes in the 1970s and 1980s (Lindmark 1978, 1979, Lonka 1981, Ruskeeniemi 1988, 1991, Sipilä 1989).

Within the frame of a new four-year battery mineral project starting in 2019, the Geological Survey of Finland reactivated investigations at the site (Kuusela et al. 2020, Al-Ani et al. 2020) and in the neighbouring Aho belt to further examine the mineral potential. The Aho belt was investigated in four target locations in Emas, Kaitåsen (Nygård et al. 2021), Dragbacken (Honka) and Kedonkangas. This report will summarize the investigations in Emas. A reservation notification for an exploration permit was made in order to protect the investigations, which included a geophysical investigation programme and two smaller drilling programmes.

2 LOCATION AND GENERAL GEOLOGY

The Emas target is located in the region of South Ostrobothnia in the municipality of Kruunupyy (Fig. 1). The closest town, Kokkola, is 40 km to the NW and has a port and railway connection. During the active investigations, GTK was granted a reservation notification (VA2019:0067) in late 2019 covering an area of 10 km^2.

The area around the river Raisjoki has been somewhat of prospective interest since the 1930s. The Emas target is in the Paleoproterozoic Pohjanmaa schist belt formation, which lies between the Vaasa granite complex and the Central Finland Granitoid Complex (CFGC). The gneissose Pohjanmaa greywacke schists are mainly intersected by N–S-trending metavolcanic sequences (Fig. 1). Along with the volcanic rocks are horizons of black schists and skarnated rock sequences with thin mafic and intermediate tuffite layers in the Aho belt (Vaarma & Kähkönen 1994). Towards the NE is the oval-shaped Veteli granodiorite, and further to the NE, bordering the CFGC, are batholites of pegmatitic granites belonging to the Seinäjoki granitic pegmatites. The grade of metamorphism in the Ostrobothnian belt rises from east to west/southwest.

The bedrock was strongly deformed during the 1860 Ma orogeneses of the Svecofennian bedrock, being thrusted into the Central Finland

Granitoid Complex. The north–south volcanic belt, together with the black schists, acted as a regional overthrust and slip/fault zone. The black schists are fine grained pelitic sulphidic graphite schists, and the graphite content varies between 3–12%. In some places, the black schist sequences may contain tremolite skarn pods and volcanic tuff interlayers a few metres wide (Vaarma & Pipping 1997). The metamorphic grade is in the lower amphibolite facies.

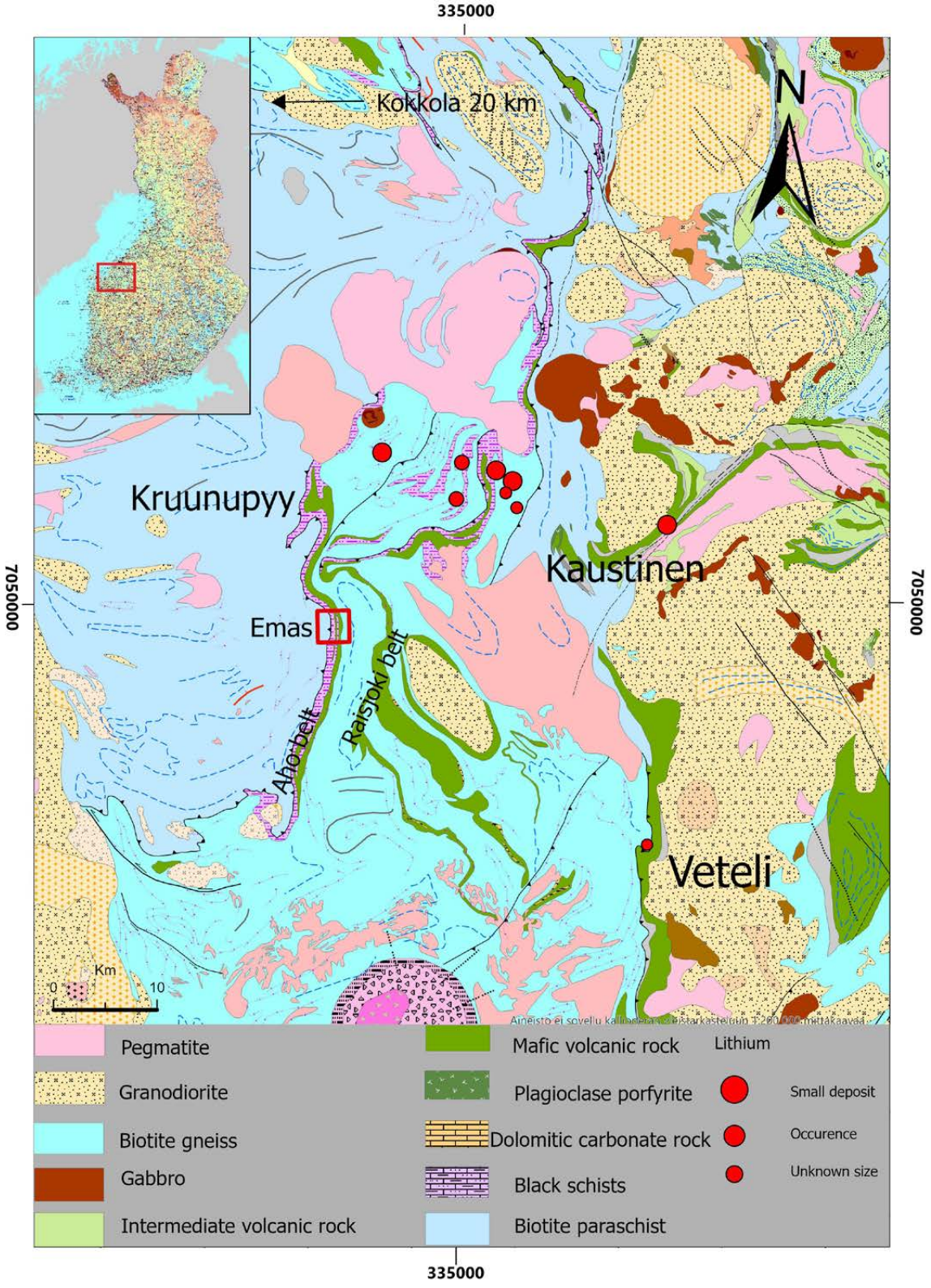

Fig. 1. Regional geological map of the area, comprising the municipalities of Evijärvi, Kruunupyy, Kaustinen and Veteli.

3 GEOPHYSICAL DATA

GTK's national aerogeophysical datasets (Hautaniemi et al. 2005), which cover the area, were used as background material for the Emas geophysical ground measurements. The flight was conducted in 2001 (flight area 275) with 200-m line spacing (EW) and a 30-m nominal altitude. The dataset consists of magnetic, frequency-domain electromagnetic (EM) and radiometric measurements.

The new surveys consist of multiple geophysical measurements, including gravity, magnetic and electromagnetic (EM) ground profiles (Table 1, Fig. 2). The measurements were conducted by GTK in separate actions between 2019–2021. The survey is still ongoing, and the rest of the EM measurements will be collected by the end of 2022.

Table 1. Survey measurement information.

Method	No. of profile lines	Line spacing	Point separation	Date
Gravity	55	50 m and 100 m	20 m and 40 m	2019–2021
Magnetic	182	50 m	1 m	2019–2021
Multi-frequency EM (MaxMin) 0.8 kHz, 3.5 kHz, and 14 kHz in-phase components	48	50 m	20 m	2019–2020

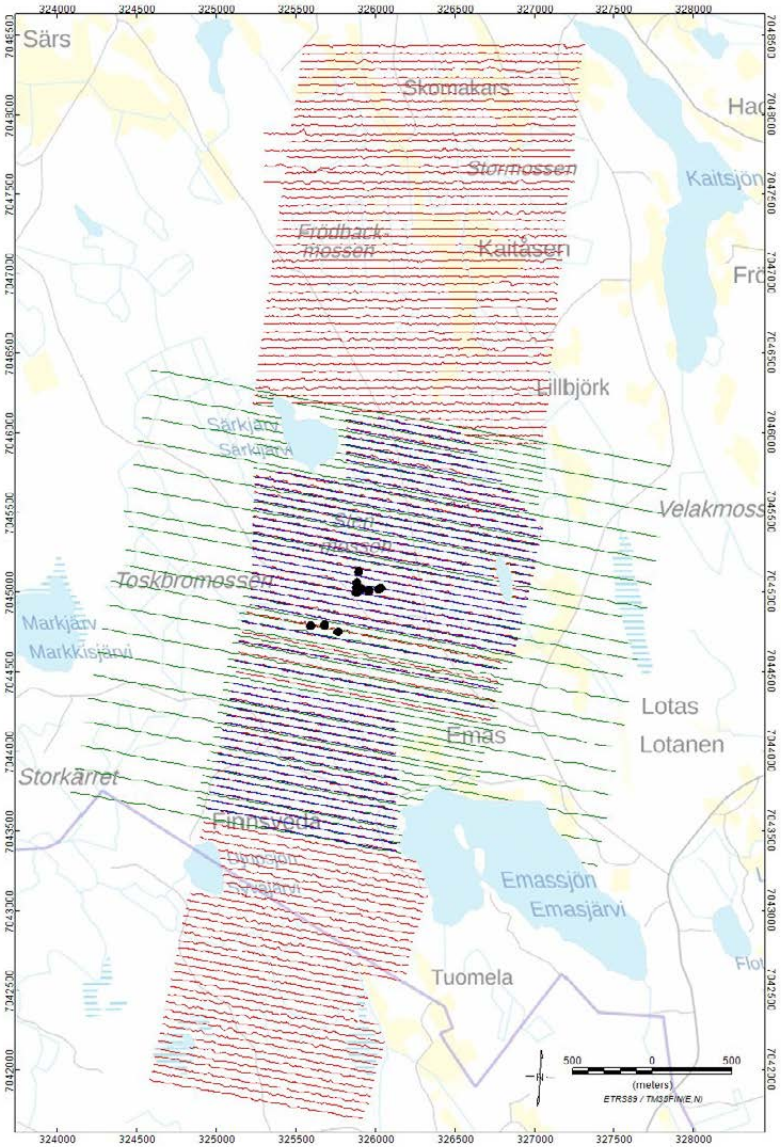

Fig. 2. Geophysical survey gravity (green), magnetic (red) and EM profiles (blue). Black dots are drill hole locations.

3.1 Gravity survey

The gravity survey was conducted in multiple sections between 2019–2021, comprising a total of 55 profile lines with 50-m line spacing. Measurements were performed every 20 m with high-precision GPS (GNSS) and a LEVA-20 hydrostatic altimeter. Gravity measurements are presented in the form of a Bouguer anomaly map, which indicates the density variations within the subsurface (Fig. 3). The gravity survey revealed a strong vertical anomaly cutting across the measurement profiles. This strong Bouguer anomaly is most likely caused by metamorphic sedimentary rocks consisting of graphite sulphide paraschist.

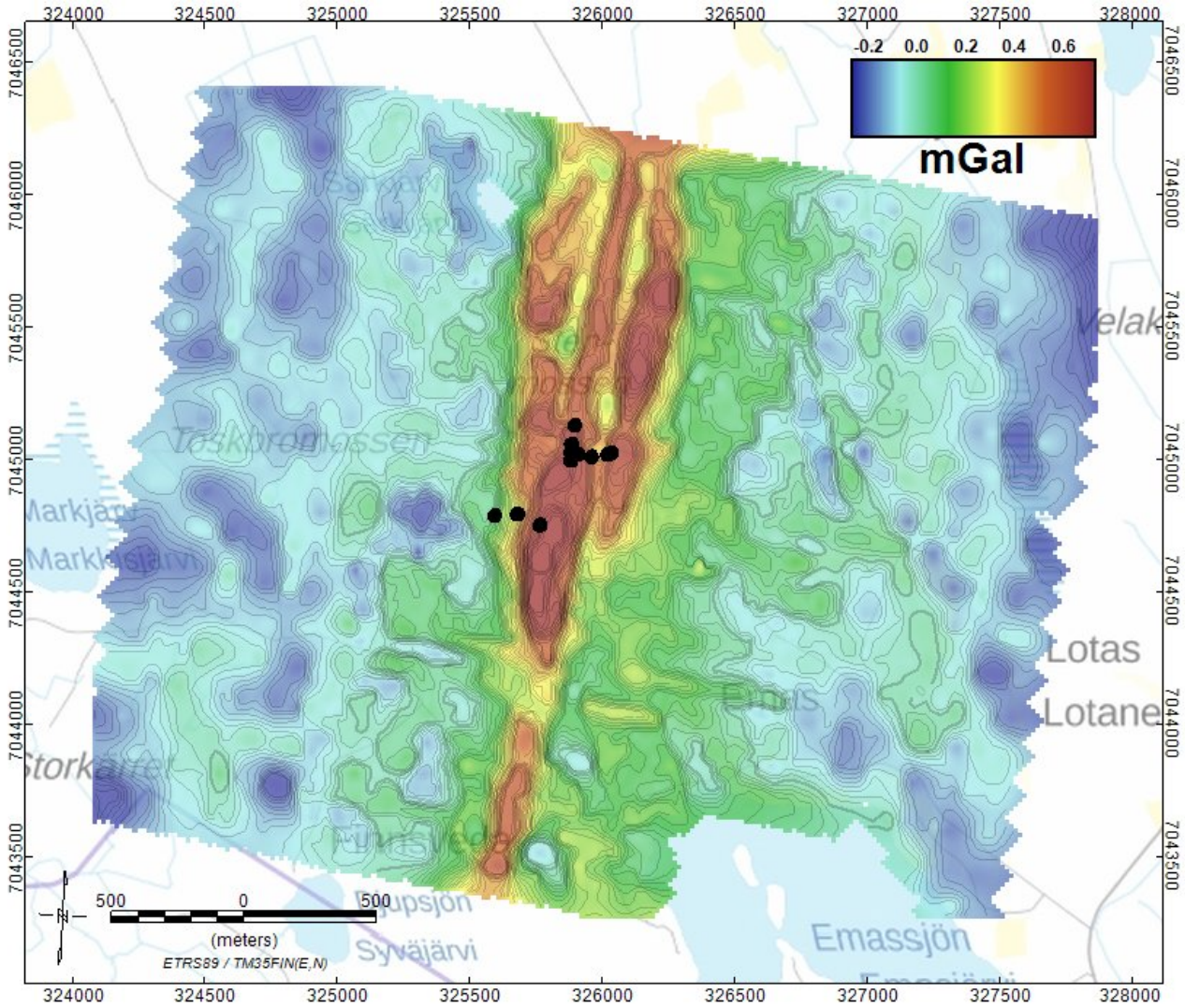

Fig. 3. The gravity survey's Bouguer anomaly map reflects the density variations. Black dots are drill hole locations.

3.2 Magnetic survey

A total of 182 magnetic ground profile lines were measured with 50-m profile line spacing between 2019–2021. Measurements were collected every 1 m with a GMS-19 Overhauser magnetometer. The magnetic anomalies present the magnetic flux density caused by the Earth's magnetic field (Fig. 4). Multiple magnetic anomalies can be observed in the survey area, with the strongest anomalies being in the west. The strongest anomalies are detected from graphite sulphide paraschist, probably caused by pyrrhotite.

3.3 Electromagnetic survey

The multi-frequency EM (MaxMin) measurements were conducted in 2019–2020. A total of 48 profiles were collected every 50 m using a slingram PROMIS FDEM system with 0.8 kHz, 3.5 kHz, and 14 kHz in-phase components. Low frequencies present the strongest electrical conductivity anomalies and have better depth penetration compared to the high-frequency in-phase components. The frequency domain method measures the electrical conductivity of the subsurface with real (Re) and imaginary (Im) components of the secondary magnetic field (Fig. 5a,b). The multi-frequency EM survey revealed interesting conductivity features that also vertically cut through the measurement lines. The conductivity response is probably caused by graphite and sulphide minerals.

All the frequencies present a strong anomaly edge at the geological contact of the biotite paraschist and graphite sulphide paraschist. In addition, the geological contact of mafic volcanic rock in between the graphite sulphide paraschist is observed as a low conductor in the northern part of the survey area. A conductive response in the northwest is only observed at a high frequency, which indicates that there is lower conductive mineralization and it most likely contains more sulphide schists than graphites. Overall, the western side of the survey area is more conductive than the eastern side, which could be caused by complex geological structures and multiple folding.

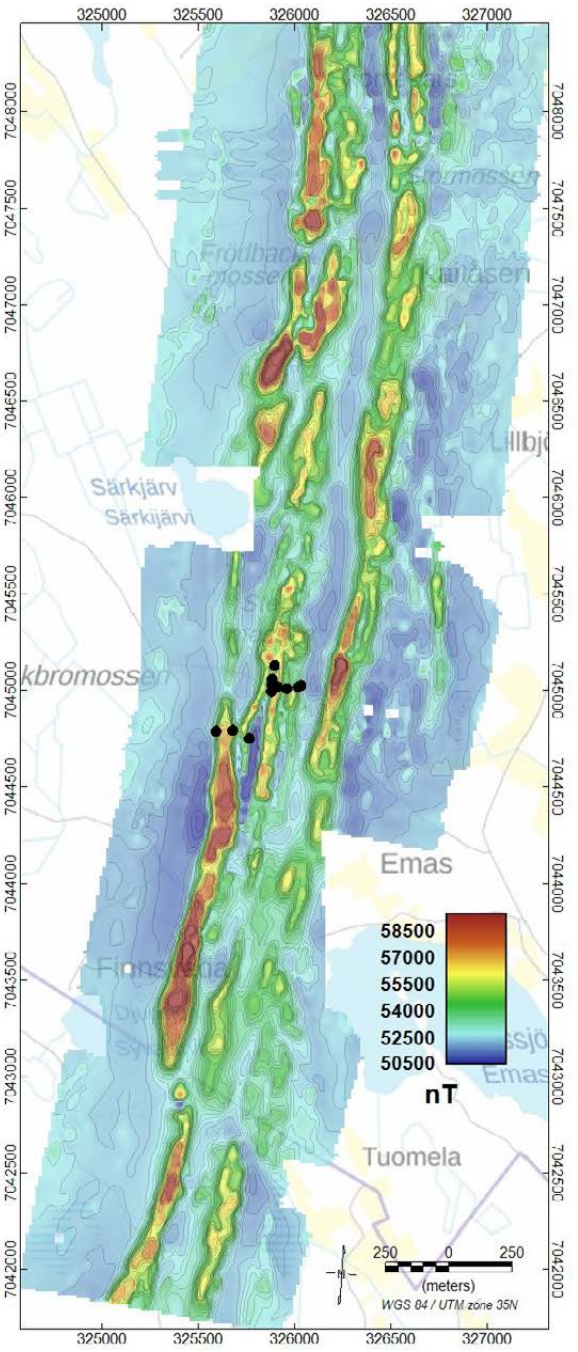

Fig. 4. A magnetic ground survey presenting magnetic components over the survey area. Black dots are drill hole locations.

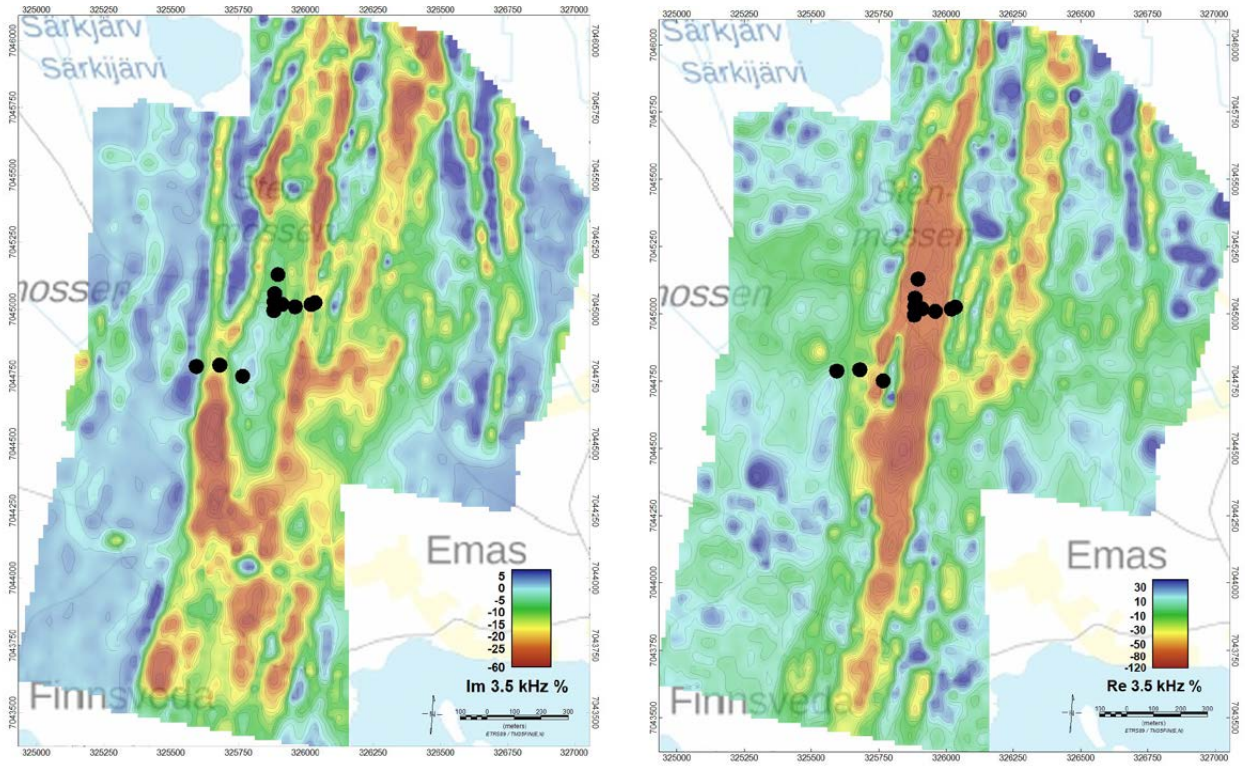

a b

Fig. 5. a) An EM survey with the Re 3.5 in-phase component, presenting the conductive objects in the subsurface. Black dots are drill hole locations. b) An EM survey with the Im 3.5 in-phase component, presenting the conductive objects in the subsurface. Black dots are drill hole locations.

3.4 Combination of survey results

A combination of geology and geophysical anomalies is presented in Figure 6. Not all the strong Bouguer anomaly areas are observed as magnetic or conductive anomalies. This can be seen in the north, where mafic volcanic rocks are surrounded by graphite sulphide paraschist. However, this area is surrounded by strong magnetic and conductive anomalies, most likely due to the graphite sulphide paraschist. Northeast of the survey area, conductive and slightly magnetic anomalies are observed, but no significant Bouguer anomaly. This could be caused by black shale and magnetite intrusions in the mafic volcanic rocks. In the southwest of the survey area, near the southern drilling locations, the graphite sulphide paraschist has a strong Bouguer anomaly and is strongly magnetic and conductive, which indicates graphite mineralization. This location could also be an indication of a fold.

3.5 Petrophysical drill hole log

GTK's petrophysical drill hole logging was conducted in the drill hole P4222019R7 (orange dot in Fig. 6). The measurements included magnetic susceptibility, electrical conductivity, density and the natural gamma ratio, and are presented in Figure 6. The drill hole is located near an area that is observed to be conductive and has a strong Bouguer anomaly, and this could be an indication of magnetite. The same indication can be seen from the drill log. Low conductivity and susceptibility are present at depths between 40–70 m, a similar pattern to that observed with normal gamma ration. The strongest susceptibility values are observed below 70 m depth.

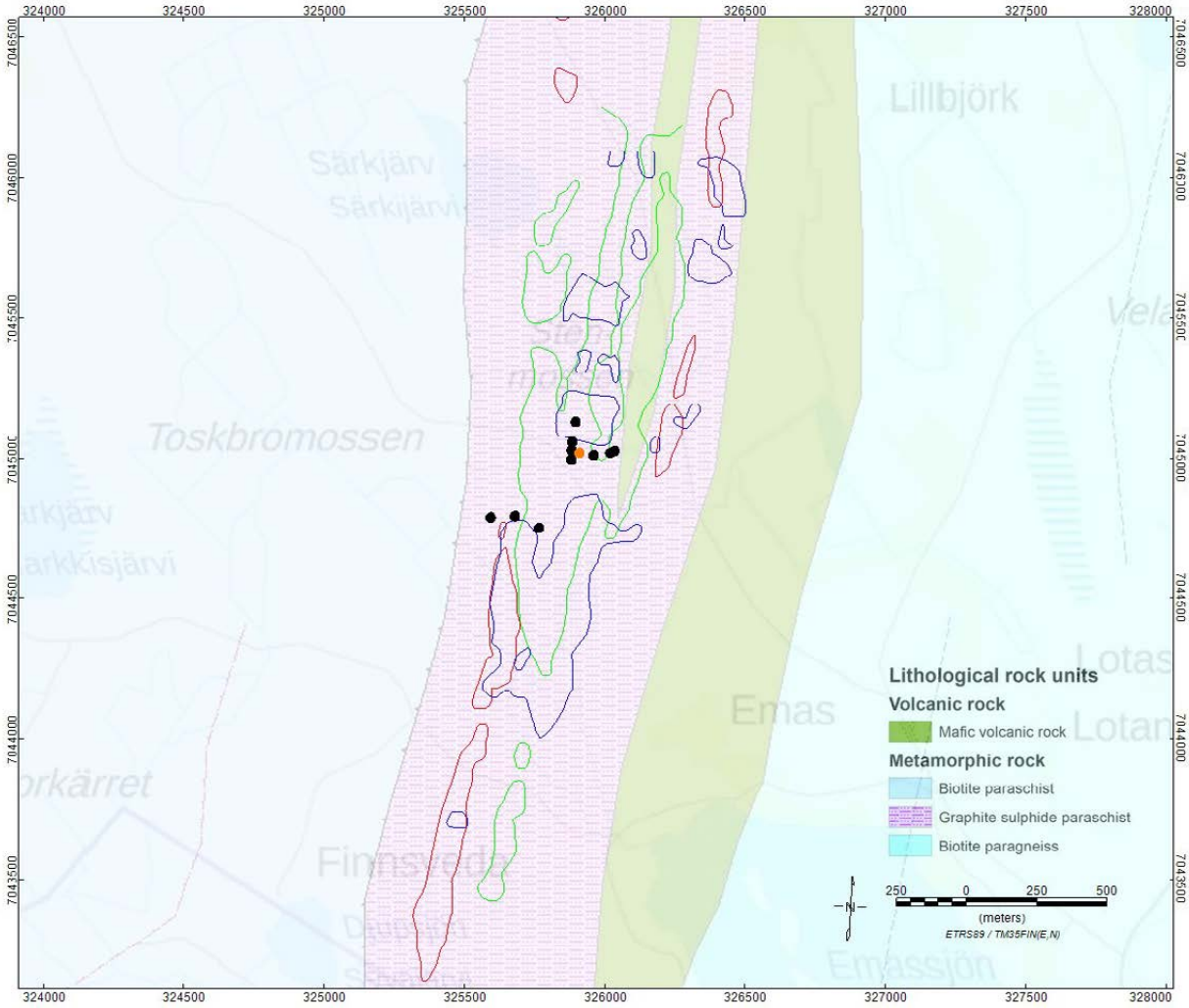

Fig. 6. Presentation of a Bouguer anomaly with over 0.5 mGal (green), magnetic properties of over 57 000 nT (red), and the EM Im 14 kHz in-phase component with less than -45% (blue) together with the geology. Black dots indicate the drill hole locations (drill hole P4222019R7 marked in orange).

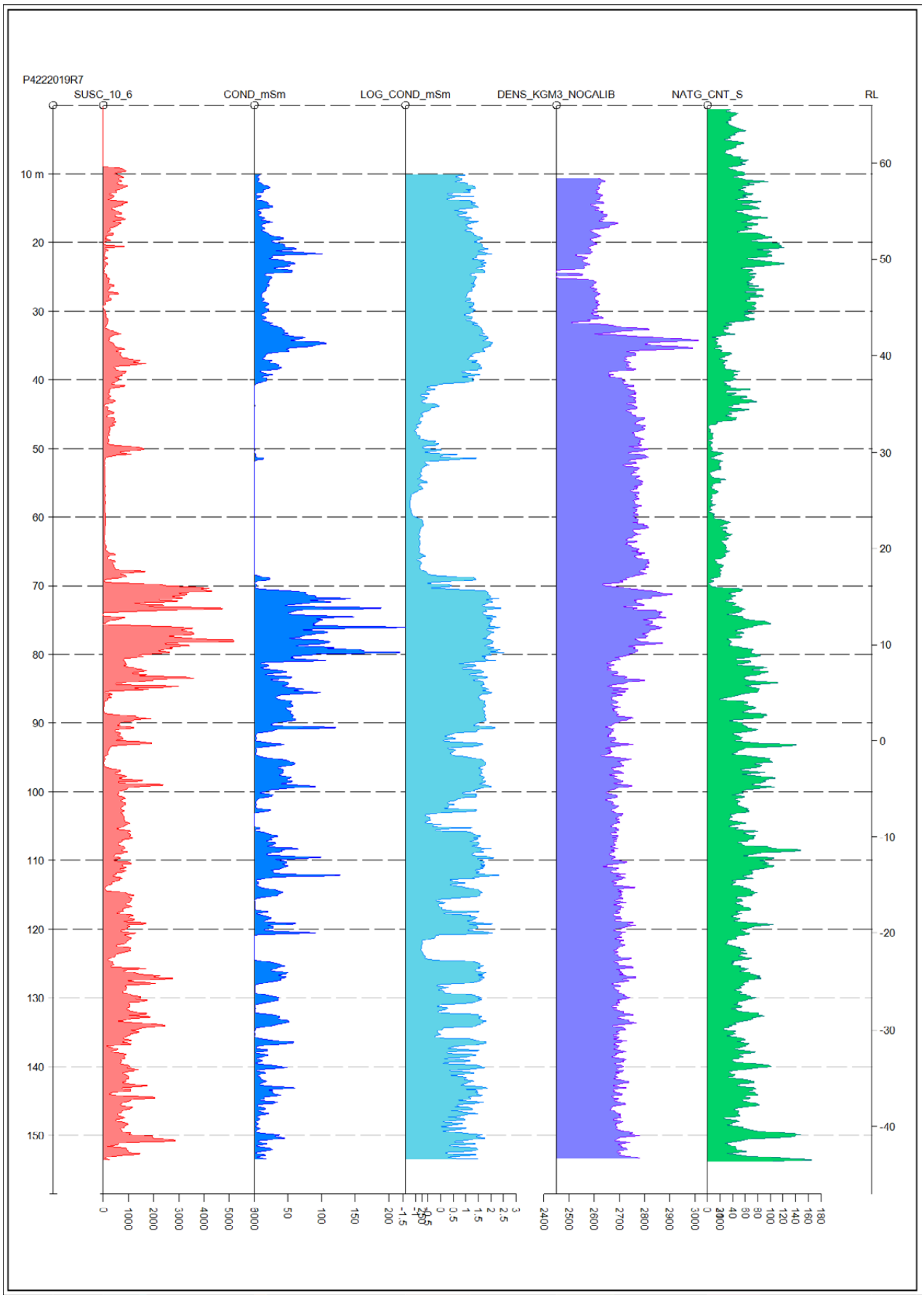

Fig. 7. GTK's petrophysical drill hole logging (P4222019R7), with measurements of magnetic susceptibility, electrical conductivity, density and natural gamma radiation.

4 GEOLOGY

After the geophysical field measurements, GTK executed a small scoping drill programme with four drill holes totalling 414.4 m. Due to the promising results, another drilling programme totalling 738.5 m was executed to trace the possible continuation of the mineralization described in chapter 5. The executed drill holes are listed in Appendix 1.

Below, a brief description is provided of the rocks encountered in the Emas drill holes, together with plots of the assay results in AFM (Fig. 10) and a volcanic rock classification diagram according to Pearce (1996) (Fig. 11).

4.1 Description of rocks

4.1.1 Amphibolite

A greenish rock often with an abundance of amphibole (actinolite) needles. The rock also contains seams of talc and biotite, as well as carbon veining. Amphibolite rocks often have an oriented appearance and appear to have undergone alteration under the influence of an ultramafic source with anomalous values of Cr, Ni and Co. According to the Pearce classification (Fig. 11), the interpreted amphibolite is classified as basalt.

4.1.2 Ultramafic rock

An ultramafic rock has by definition high MgO and FeO and low K, which is well in accordance with the rock type encountered in Emas. The ultramafic rock is light grey in colour, massive, talc rich, and often has clear contacts to surrounding rocks. A typical feature is also that the rock contains high Cr values (Fig. 21).

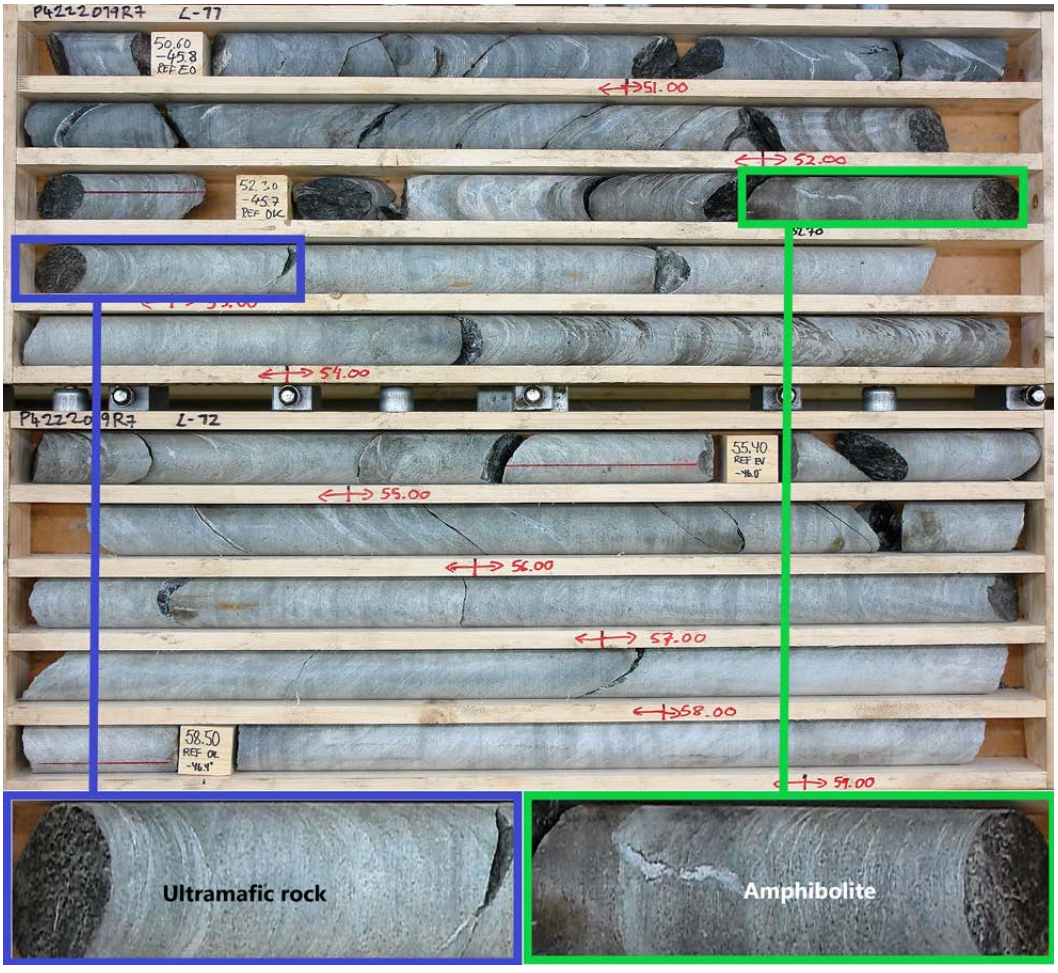

Fig. 8. The contact zone of amphibolite and ultramafic rock in drill hole R7.

4.1.3 Volcanic rock

Contains a wider array of rocks, of which the majority are greyish, even grained or described as massive, varying from intermediate rocks of a rhyolite dacite composition to a slightly greenish, more mafic (andesitic) rock type (Fig. 9). Intertwined with graphite-rich (turbidite) sections are often found volcanic tuff layers with organized layering, but also unorganized mass-flow textures.

4.1.4 Black schist

Dark grey to black, often with substantial amounts of graphite and pyrrhotite and some pyrite in thicker sections. Black schists are often present as thin layers in rocks logged as volcanic rocks (Fig. 9), which can be seen as a rise in the overall U-content in the whole rock assays.

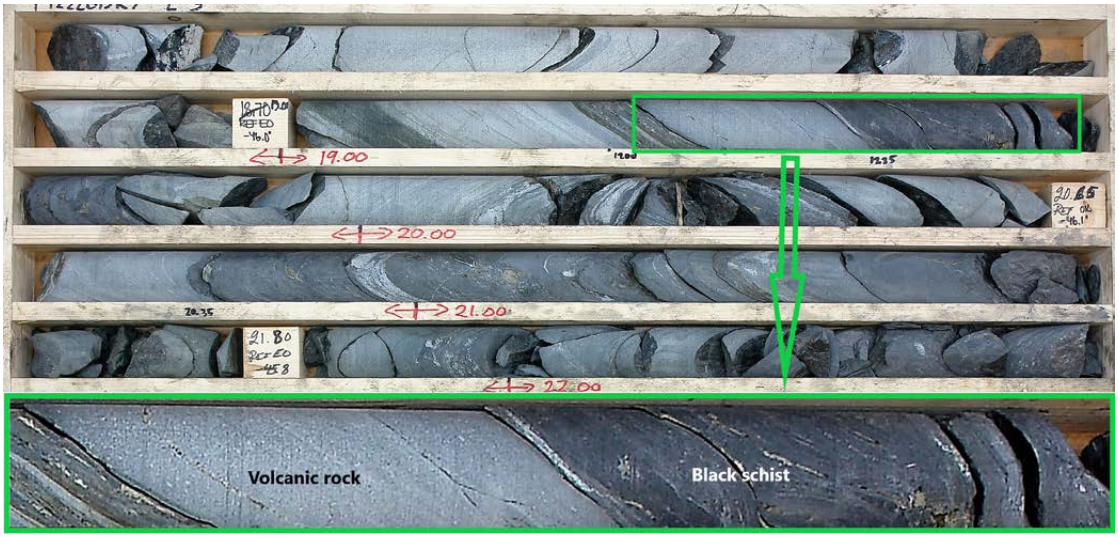

Fig. 9. Drill core box from drill hole R7. Black schists are often intertwined with volcanic tuff layers.

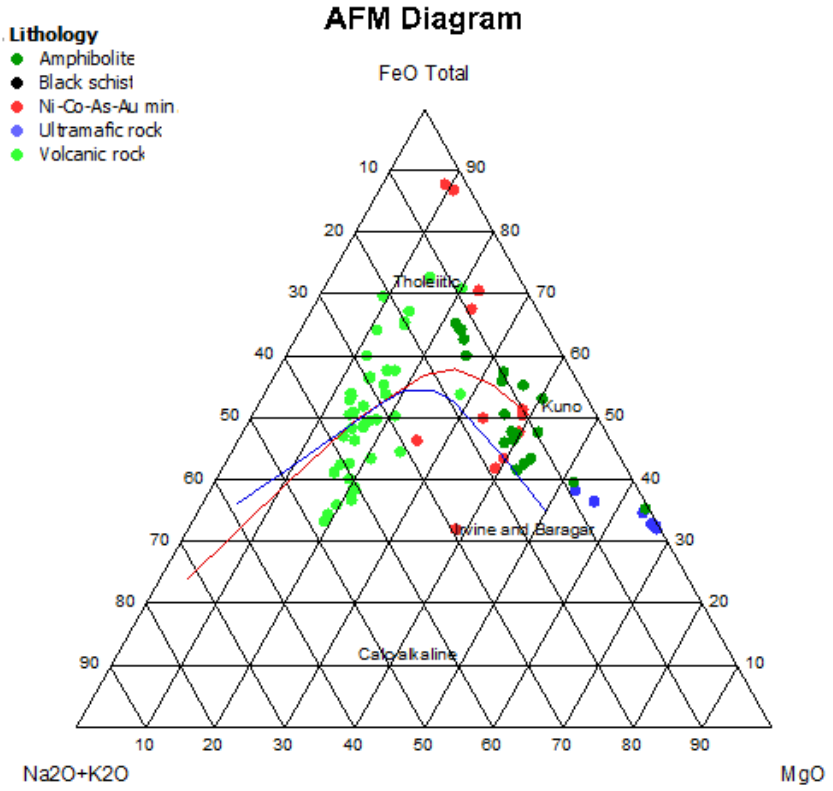

Fig. 10. An AFM diagram of the Emas rocks.

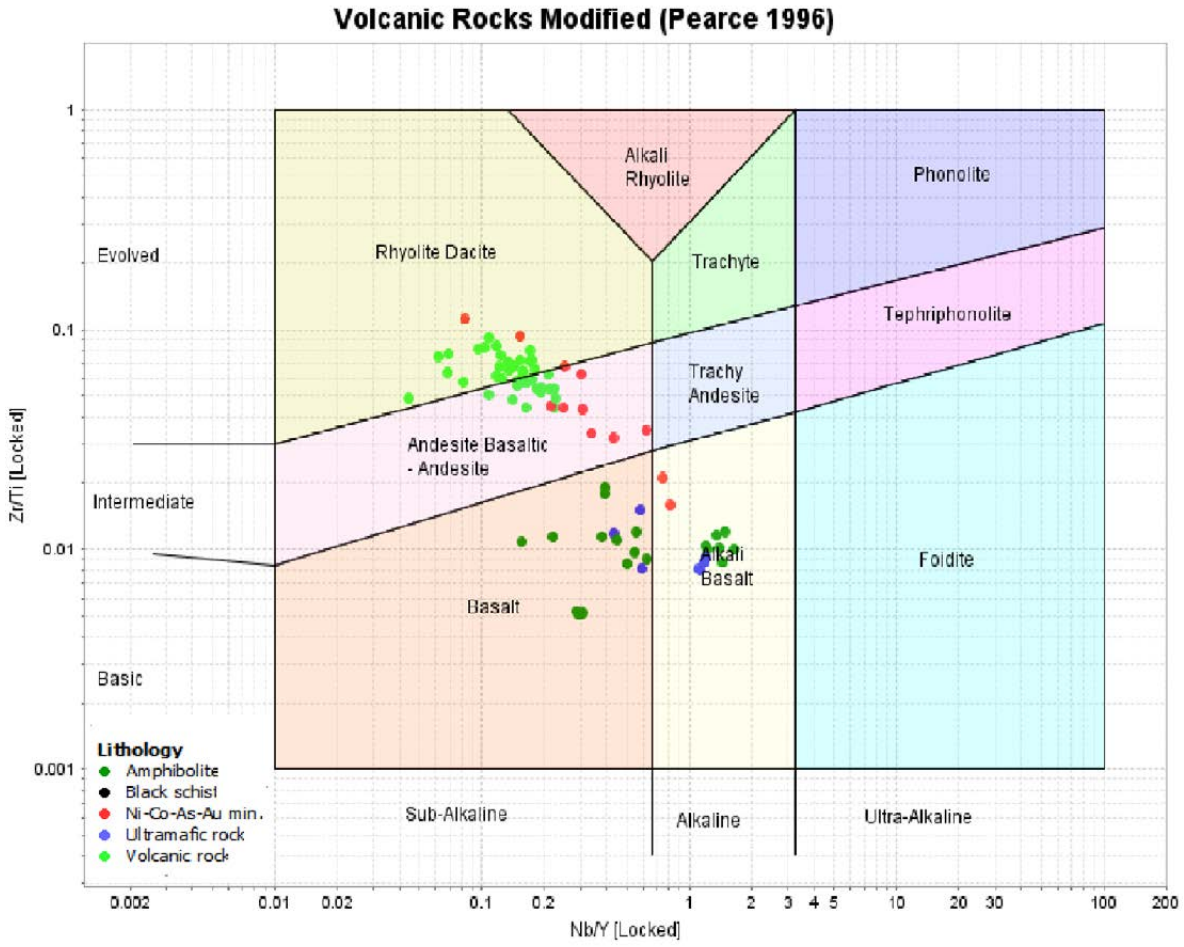

Fig. 11. Rock classification based on the Emas assay results according to Pearce (1996).

4.2 Structural geological overview

The Emas area is a part of a 30-km-long N–S-trending volcanic belt known as the Aho belt (Fig. 12). A very similar belt occurs in the east, referred to as the Raisjoki belt. In the Kaustinen area, spodumene pegmatites are closely associated with the volcanic rocks (Kuusela et al. 2011, Ahtola et al. 2015).

Multiple generations of deformation can be recognized in southern and central Ostrobothnia. Thrusting is considered by Vaarma et al. (1997) being one of the earliest deformations stages and has brought the Aho and Raisjoki belts to their present locus. A thrust fault between the sulphide graphite schist and Lappfors suite metagreywacke, and between the metagreywacke and the Pirttikylä suite mica gneiss is presented in the bedrock map (Fig. 1; Bedrock of Finland – DigiKP).

The surroundings of the Emas target lack outcrops, but further south, in the Mansikka-aho area, outcropping rocks have recently been structurally overviewed from microscopic to cartographic scales with three visible recognizable foliation trends (Lehto 2021). The presence of a NE-trending shear, also interpreted as regional open folding (Lehto 2021), can be followed as continuous aeromagnetic negative anomalies (Fig. 12). The large-scale bended folded “hooks” in the northern and southern parts of the Aho formation could be a result of large-scale strike-slip shear movements along the limbs of the open folds.

The modelled drill holes (Fig. 12) according to the identified lithologies are steeply dipping to the east and west. This feature is shown in the model based on core measurements. The structural measurements are presented in a stereographic plot (Fig. 12) and illustrated in a block model in Figure 12.

Measurements were taken from the core wherever possible after each drill run of 3 metres. It is worth noting that local folds might remain unnoticed, since the measurements are not continuous along the core. Bedrock folds, especially in the black schist, often coincide with brittle shear zones.

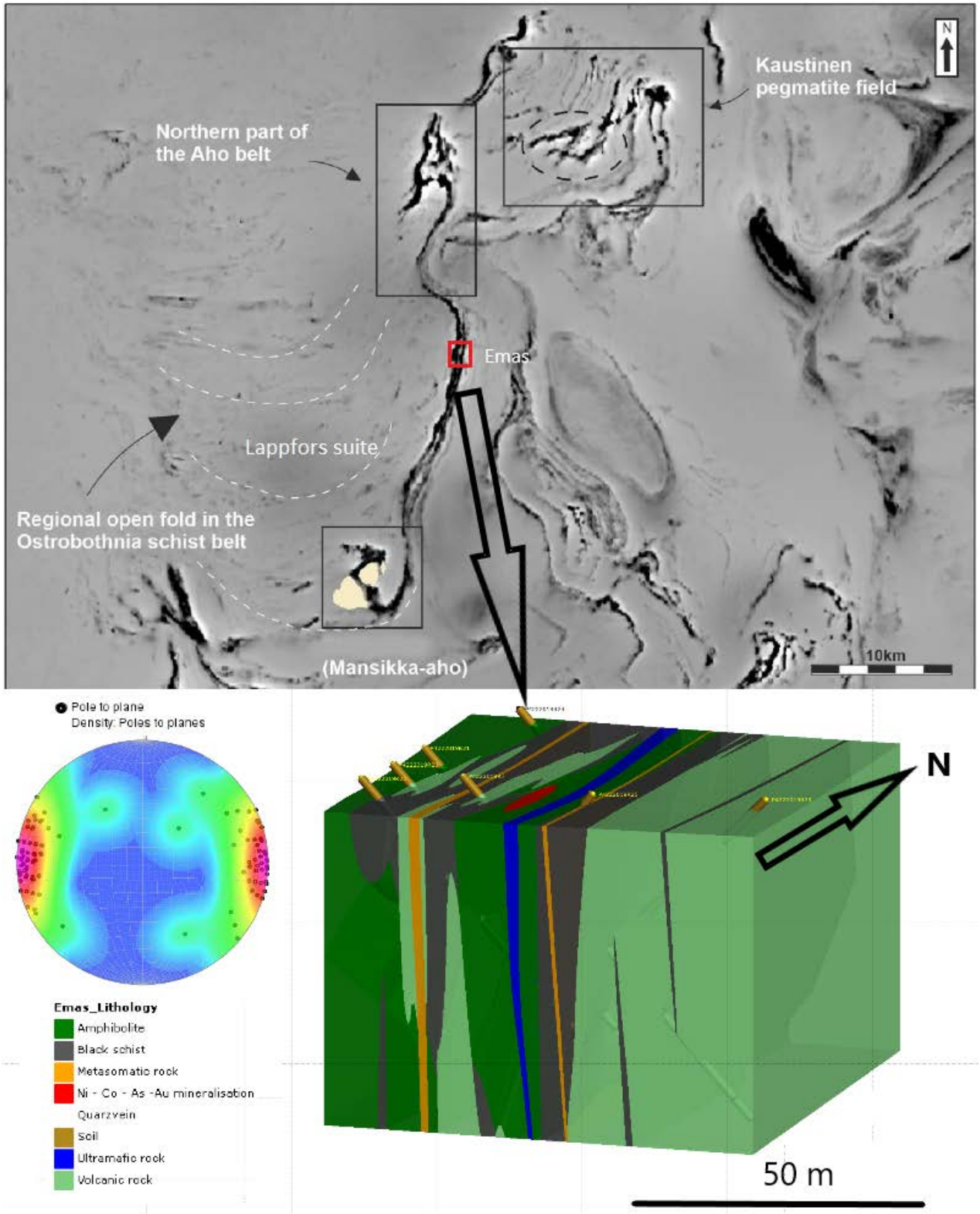

Fig. 12. A magnetic map (above) modified from Lehto (2021) to illustrate regional-scale structures, with a block model and stereoplot of the measured foliation directions in the Emas drill core.

4.3 CT scans of Emas drill core samples

Two samples from the Emas drill core were scanned with a CT scanner. The device was a GE phoenix, which can perform X-ray computed microtomography (µ-CT) and create images of the interior of solid materials, such as rocks, in 3D for any orientation. The initial aim of the CT scans was to investigate whether the CT scanner could visualize the flake-size distribution from drill core size samples to be used as an estimation or even a replacement tool for thin sections in the first-stage quality assessment of graphite. Knowledge of the flake-size distribution is valuable in the beneficiation process.

The samples were scanned using the 240 kV microfocus tube. At each angle, the detector waited for a single exposure time and then took an average of over three exposures. No ring artifact reduction was used for any of the samples in reconstruction. Some samples were scanned as a vertical multi-scan, combining more than one scan for the final result.

The flake size could not be estimated from the performed scans, but instead, the CT images were shown to visualize two graphite-rich schists that appeared 10 m and 100 m from the main sulphide mineralization. Shear deformation is evident in sample R7 23.70 (Fig. 13a), displaying a multitude of lineament directions, with the sulphide solutions intruded into the fractured spaces. In this sample, there is an elevated content of Zn and U, which is usually closely associated with a high graphite content. The second sample, 153.60, logged as a graphite-rich volcanic rock, displays a clearly less disturbed texture (Fig. 13b).

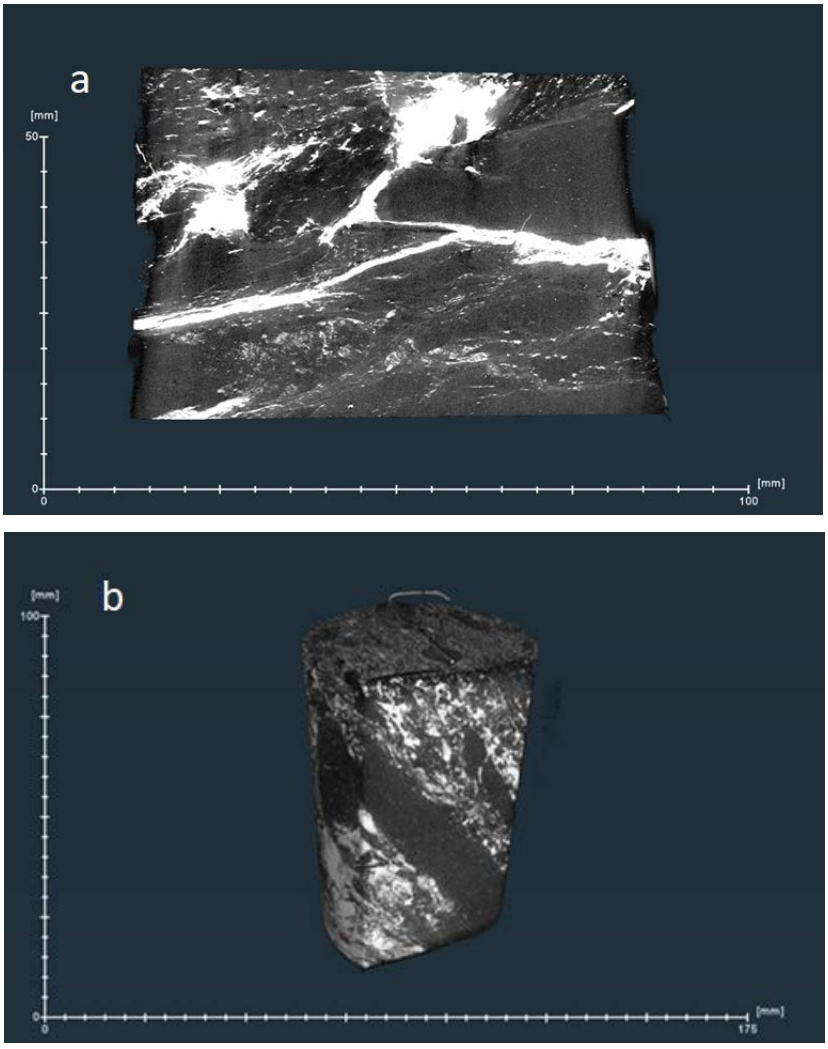

Fig. 13. a) Sample 23.70 from drill hole R7 displays mineralized fracture networks caused by shearing in a black schist located 10 m from the Ni–Co–Au mineralisation. b) A sample from drill hole R7 153.70 m, displaying graphite-rich volcanic rock less affected by shearing.

5 ORE GEOLOGY

5.1 Sulphides

In the first drilling programme, comprising four drill holes totalling 414.4 m, a 10-m-wide differentiation zone was penetrated in drill hole R7, containing a 2-m-wide semi-massive sulphide mineralization (Figs. 15 and 17). The analysis results included 3 m @ 0.5% Co with 2% Ni or 10.5 m @ 0.8% Ni with 0.11% Co. The semi-massive section also contained 0.32 ppm Au in a 2.15-m section. Minerals identified in the semi-massive sulphide zone included Ni-rich pyrite, pentlandite, gersdorffite and cobaltite. Due to the promising results, another drilling programme totalling 738.5 m was executed to trace the possible continuation of the mineralization. In the second drilling campaign, the continuation of the differentiation zone could be localized with low-grade results according to Figure 14, but no semi-massive mineralizations were penetrated in the second campaign drill holes.

5.2 Graphite

The drilling programme penetrated several graphite-rich black schist layers (C graphite >1% and S >1%) flanking the mineralized Ni–Co–Au zone on both sides (Fig. 14, plan view). In the later analysis batches, graphite was analysed, yielding several sections of 7–15 m @ 7% Cg (Table 3, Fig. 16). The graphite-rich layers are often associated with a rise in U and Zn contents. Alternating graphite layers within the volcanic rocks make the rock incoherent, resulting in a fractured drill core. As the U content suggests in Figure 21, the volcanic rock contains multiple sections of intercalating graphite layers below 70 m in drill hole R7.

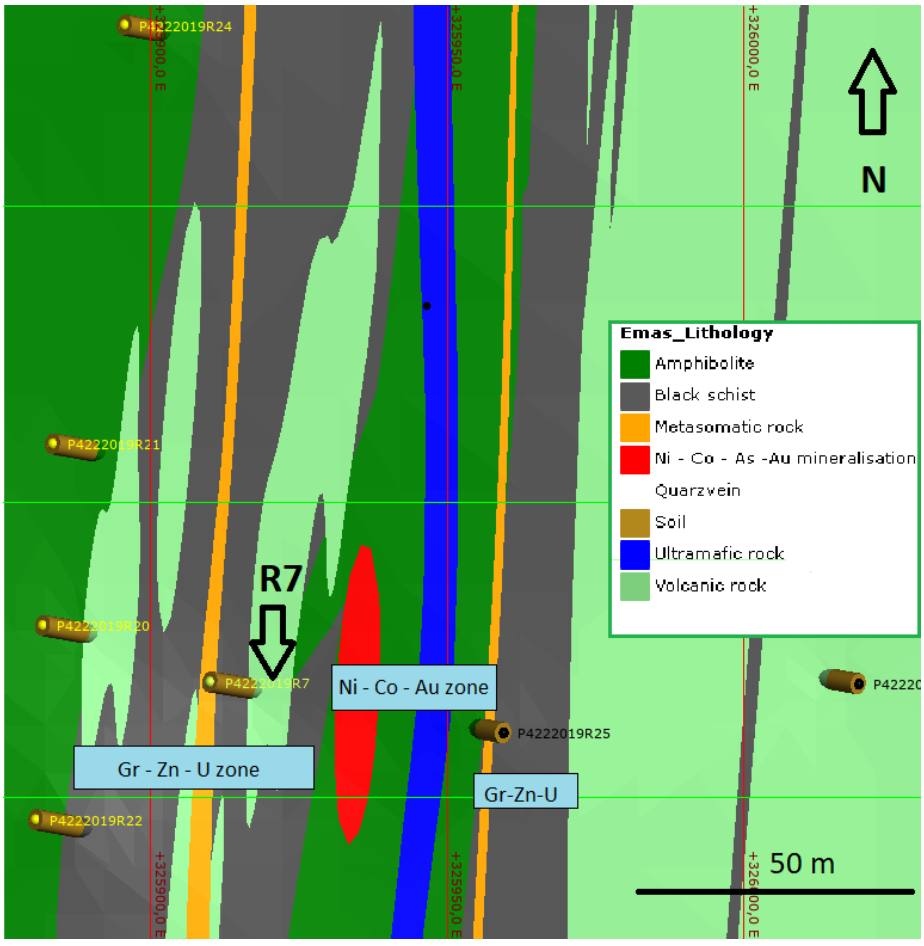

Fig. 14. Plan view of a geological map indicating the locations of drill holes R7–R25 with mineralized zones. Graphite-rich black schists occur on both sides of the Ni–Co mineralized amphibolitic and ultramafic rocks.

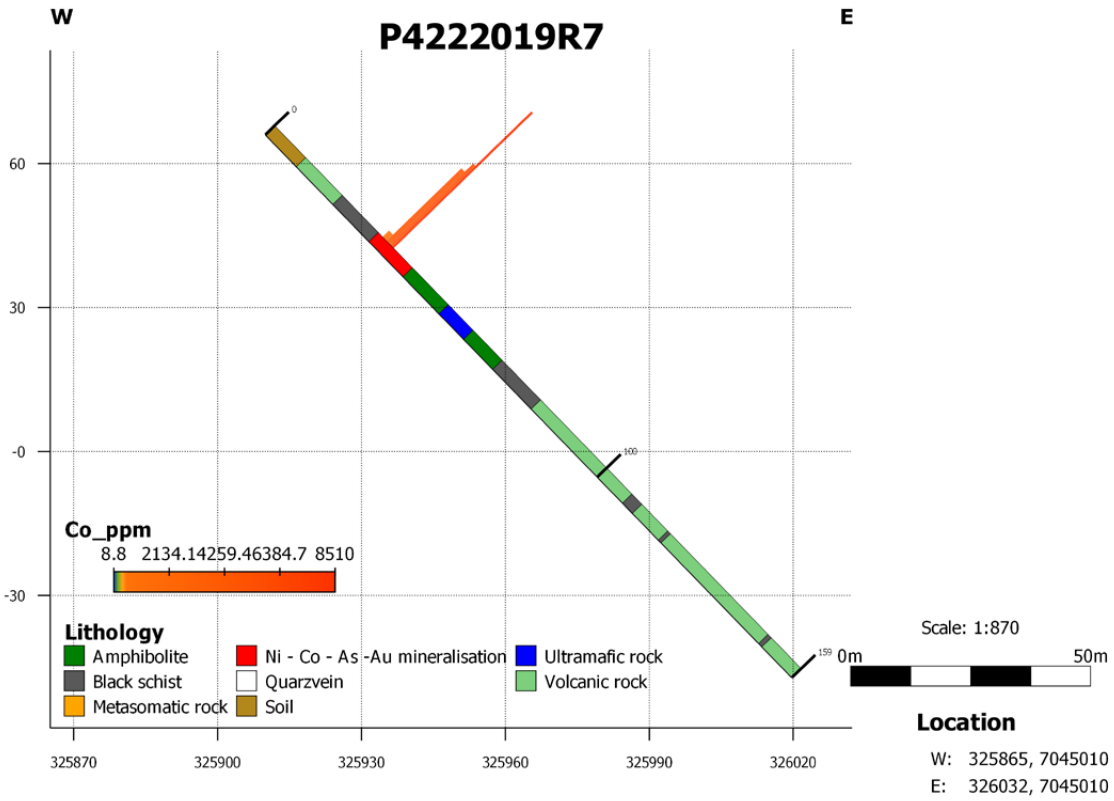

Fig. 15. Cross-section of drill hole R7 with a Co-rich mineralized zone of 3m @ 0.5% Co with 2% Ni and a 2m section of 0,32ppm Au.

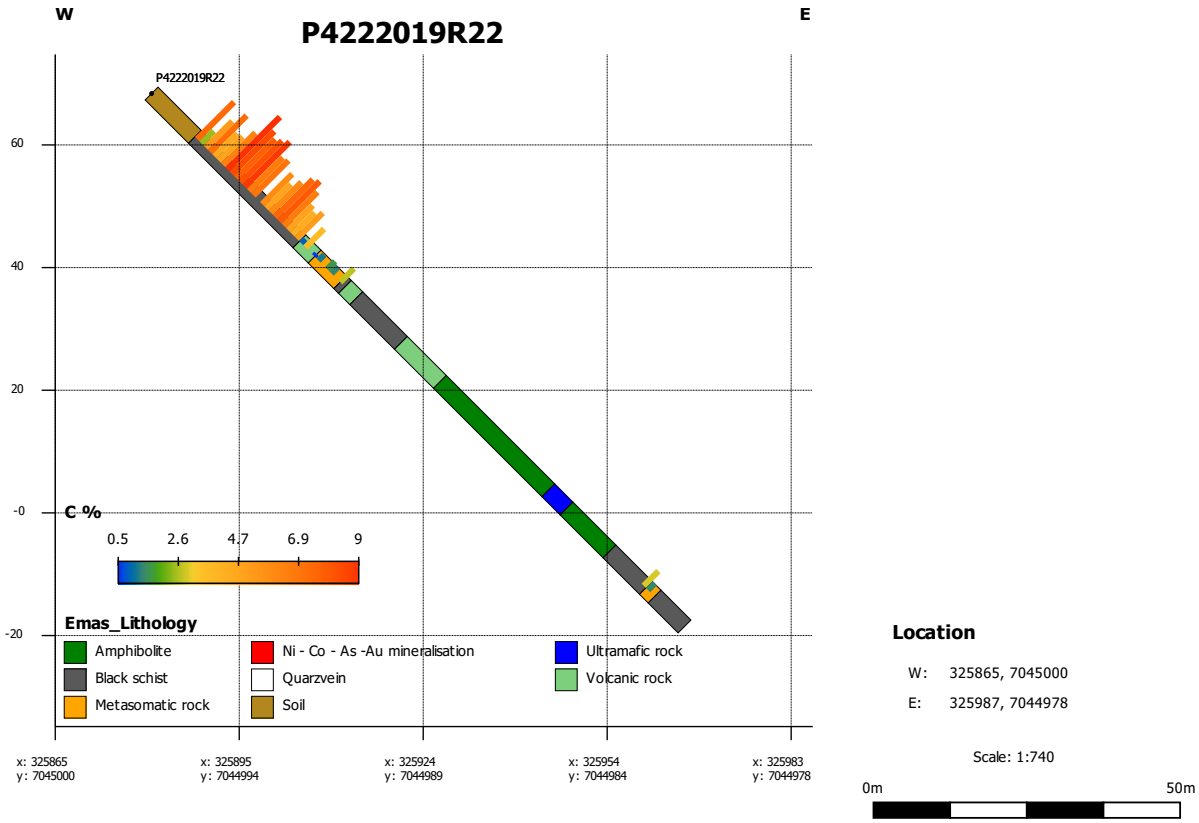

Fig. 16. Cross-section of drill hole R22 with a flake graphite section up to 15 m wide with an average of 7.2% Gr.

5.3 Assay

A total of 299 drill core samples from Emas were analysed at Eurofinns Labtium with the method 306PM (ICP-OES/ ICP-MS) covering 53 elements. Additionally, 121 samples were analysed using a C-analyser and 52 samples for Au with ICP-OES method 703P.

Table 2. Maximum, median and minimum values of assay results from selected elements in Emas drill core. The max values of Ni, Co, Cr, Au, As are obtained from the main mineralized zone whereas C, U, Zn max values are from black schists.

Element	Max	Median	Min
Co_ppm	8510	42.7	4.1
Ni_ppm	40 100	239	25
C_%	12.6	5.2	0.47
Au_ppb	501	10	10
Zn_ppm	2420	175	23
Cr_ppm	2450	151	8
As_ppm	44 900	25.1	1.14
Fe_ppm	346 000	95 400	27 700
V_ppm	1050	277	36.2
U_ppm	35.6	4.29	0.2

Table 3. Drill hole intersections according to the content of Co, Ni, Au and flake graphite.

Drill hole	From (m)	To (m)	Intersection (m)	Element	content
P4222019R7	32.5	43	10.5	Co	0.11%
P4222019R7	32.5	43	10.5	Ni	0.8%
P4222019R7	33.7	35.85	2.15	Au	0.32 ppm
P4222019R20	32	39	7	Cg	7.3%
P4222019R21	35	43	8	Cg	7%
P4222019R21	98	114	16	Co	102 ppm
P4222019R21	98	114	16	Ni	0.095%
P4222019R22	16	31	15	Cg	7.2%
P4222019R22	66	84	18	Co	176 ppm
P4222019R22	66	84	18	Ni	0.18%
P4222019R24	20	28	8	Cg	7.1%

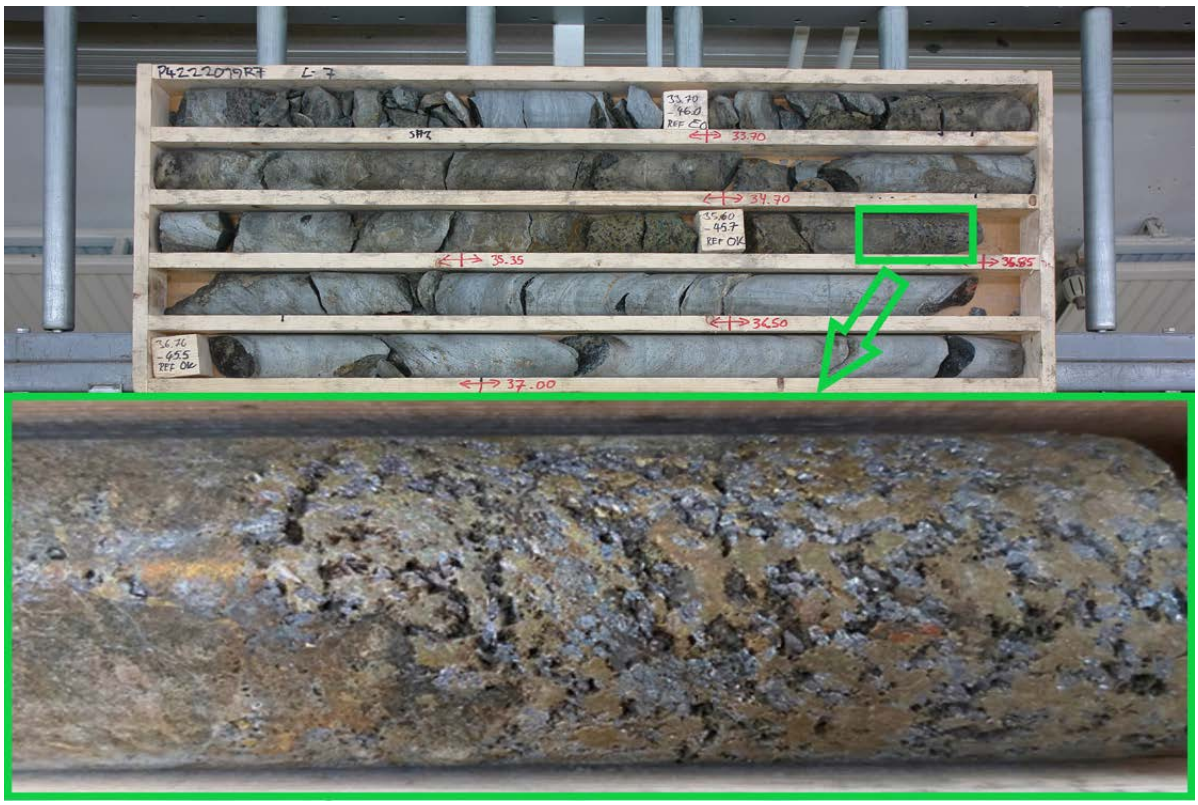

Fig. 17. A massive section of Ni–Co–As, comprising 3 m @ 0.5% Co with 2% Ni and 2 m 0,32 ppm Au. The minerals identified in this melange are gersdorffite, pentlandite, cobaltite and As-rich pyrite.

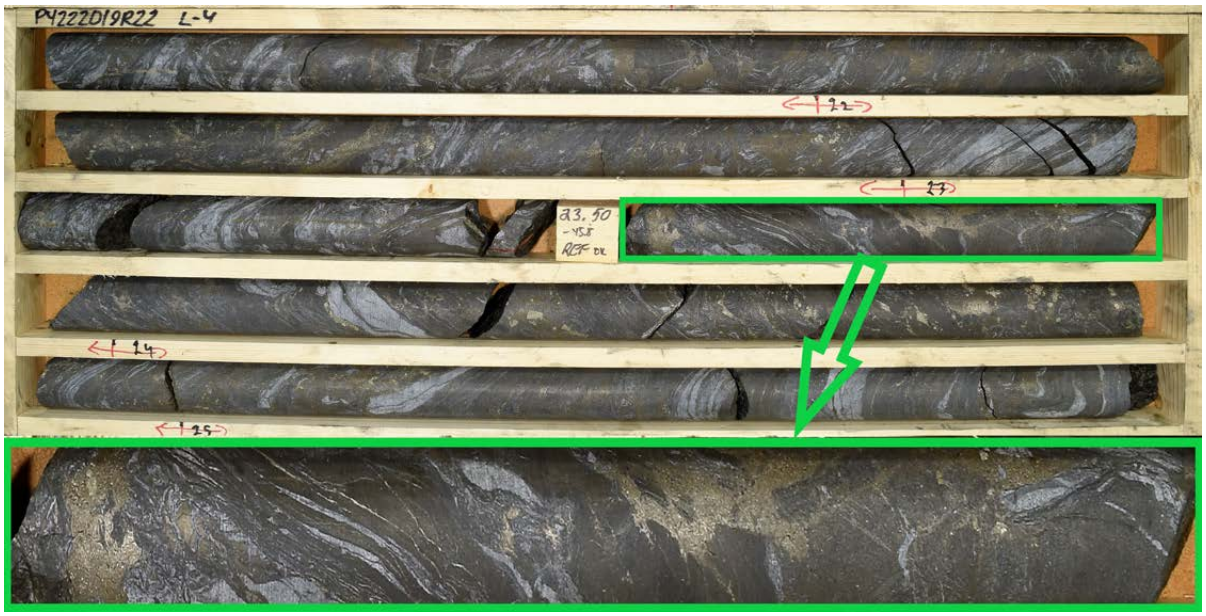

Fig. 18. A part of Emas black schist section 16–32 m from drill hole R22 with an average flake graphite content of 7.2%. The present sulphides are dominated by pyrrhotite and pyrite.

5.4 Correlations plots

Correlation plots based on drill hole assay results were drawn with the ioGas program to visualize factors that appear to have affected the mineralization and could work as pathfinders in tracing these mineralization types.

5.4.1 Flake graphite

The black schists are easily traceable from airborne geophysics. The challenge is to determine whether the graphite-rich layers contain lesser contents of 1–4% graphite or more prospective contents of >4%. The flake graphite-rich layers in the Emas area and most likely the whole Raisjoki investigation area have a regularly anomalous content of U and somewhat also of Zn (Fig. 19b) associated with the graphite layers, allowing especially radiometric content measurements as another means to estimate the flake graphite content. In a robust estimate, a rise in the U content in Emas correlates generally well with a rise in the graphite content, especially if the graphite content is above 4% (Fig. 20).

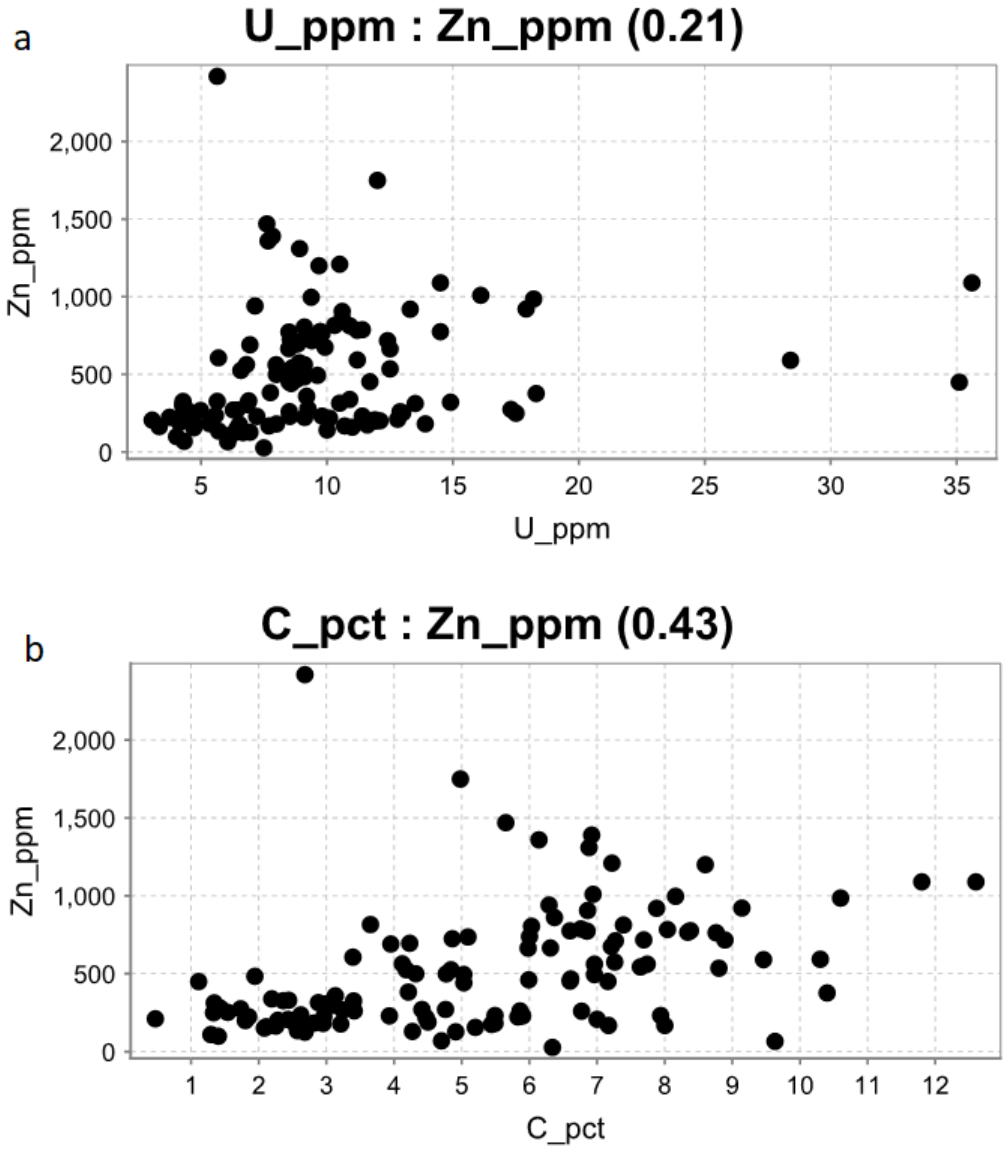

Fig. 19. a) and b) Assay results-based correlations of C with Zn and U with Zn.

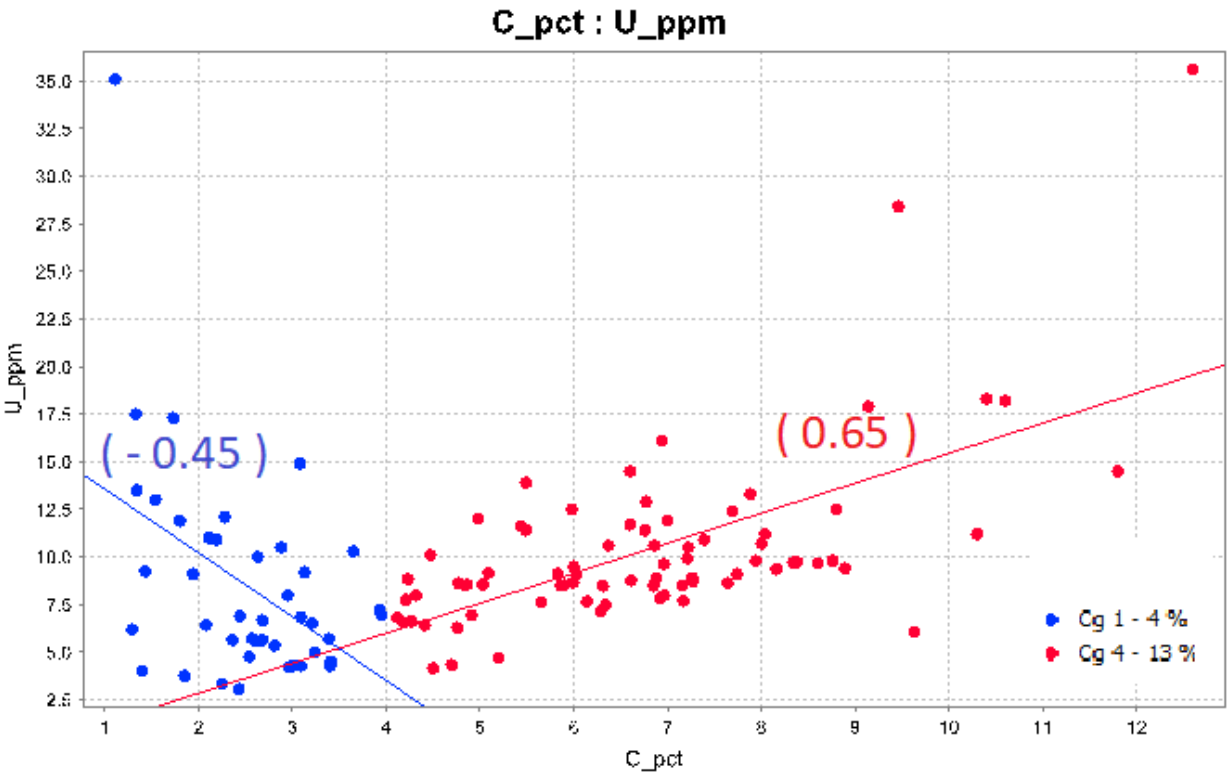

Fig. 20. Correlation between two sample populations based on the graphite content in Emas black schists. Graphite (C) correlates well with U if Cg > 4% in 78 samples (red population), but correlates poorly with U if Cg < 4% in 42 samples (blue population). Note that high U-values are not excluded if the graphite Cg < 4%.

5.4.2 Co–Ni–Au mineralization

The Co–Ni–Au mineralization is clearly affected by augmented Cr (Fig. 21), and this relation can be observed in every drill hole intersection with anomalous Ni–Co (Table 3). The amphibole-rich volcanics logged as amphibolite have an ultramafic core. Arsenic correlates well with Ni–Co and has probably also functioned as an Au carrier.

Table 4. Correlation matrix of most base metals in the Emas sulphide mineralization from 78 samples, where Cg > 4%. Zn also correlates better with U with an increased C content.

Correlation	C_pct	Zn_ppm	U_ppm	Co_ppm	Ni_ppm	S_ppm	Pb_ppm	Fe_ppm	Cu_ppm	As_ppm	Au_ppb
C_pct	1	0.32	0.65	0.2	0.34	0.079	0.5	0.077	0.17	-0.041	
Zn_ppm	0.32	1	0.65	-0.069	-0.085	0.41	0.52	0.37	0.19	-0.052	0.093
U_ppm	0.65	0.65	1	-0.12	-0.16	0.51	0.71	0.34	0.28	-0.093	0.22
Co_ppm	0.2	-0.069	-0.12	1	0.95	0.38	0.02	0.15	0.43	0.98	0.17
Ni_ppm	0.34	-0.085	-0.16	0.95	1	0.36	-0.002	0.14	0.29	0.93	0.18
S_ppm	0.079	0.41	0.51	0.38	0.36	1	0.53	0.8	0.51	0.39	0.33
Pb_ppm	0.5	0.52	0.71	0.02	-0.002	0.53	1	0.46	0.33	0.034	0.63
Fe_ppm	0.077	0.37	0.34	0.15	0.14	0.8	0.46	1	0.43	0.15	-0.084
Cu_ppm	0.17	0.19	0.28	0.43	0.29	0.51	0.33	0.43	1	0.34	0.43
As_ppm	-0.041	-0.052	-0.093	0.98	0.93	0.39	0.034	0.15	0.34	1	0.79
Au_ppb		0.093	0.22	0.17	0.18	0.33	0.63	-0.084	0.43	0.79	1

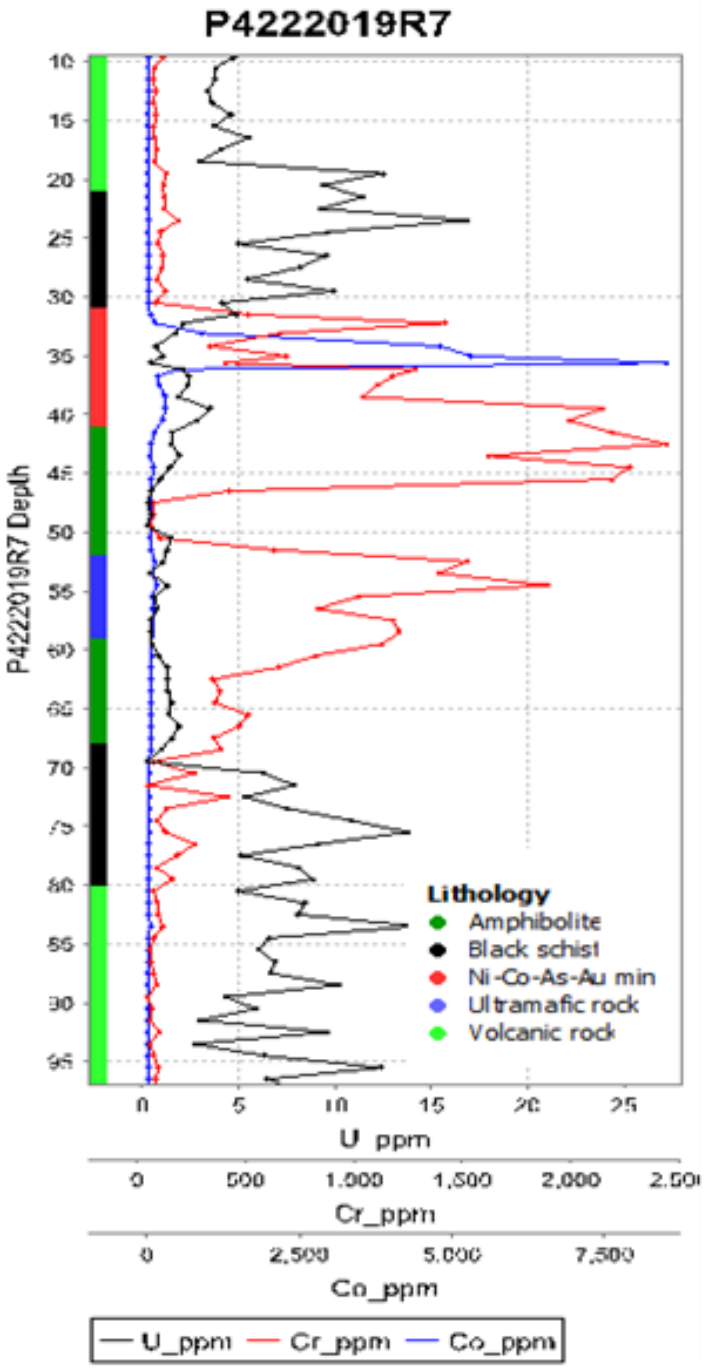

Fig. 21. Element correlation in a downhole section of drill hole R7. The rise in Cr enveloping the Ni–Co–As–Au mineralisation suggests an ultramafic source driving the Ni–Co–As–Au enrichment.

6 SURFACE GEOCHEMICAL SURVEY

A surface geochemical survey was performed in the Emas target area in 2020. Altogether, 144 samples were collected from 138 sample sites (Fig. 22) (Hulkki 2022). The sampling was carried out as line sampling consisting of six lines with a sample spacing of 10–50 m. For sampling, small pits were dug with a shovel (depth 30–40 cm) and the samples were collected from the B horizon. The laboratory of ALS Finland Oy provided the analyses. The chemical analysis method used was a modified aqua regia digestion (1:1 HNO3:HCl) in combination with low detection limit ICP-MS. Altogether, the concentrations of 65 elements were determined.

In the Emas target, a Ni–As–Co–Cu mineralization has been detected by diamond drilling (drill core P4222019R7). The distribution of the mineralization-related elements Co, As, Cu and Ni is presented in Figure 23. The concentration of Co was also classified into different categories, where the anomalous concentrations were separated from the background using a threshold value. The threshold value was determined using a log-transformed Tukey boxplot, in which the threshold between the anomaly and the background was determined with the formula Q3 + (1.5 x IQR), where IQR = Q3-Q1 (Carranza 2009).

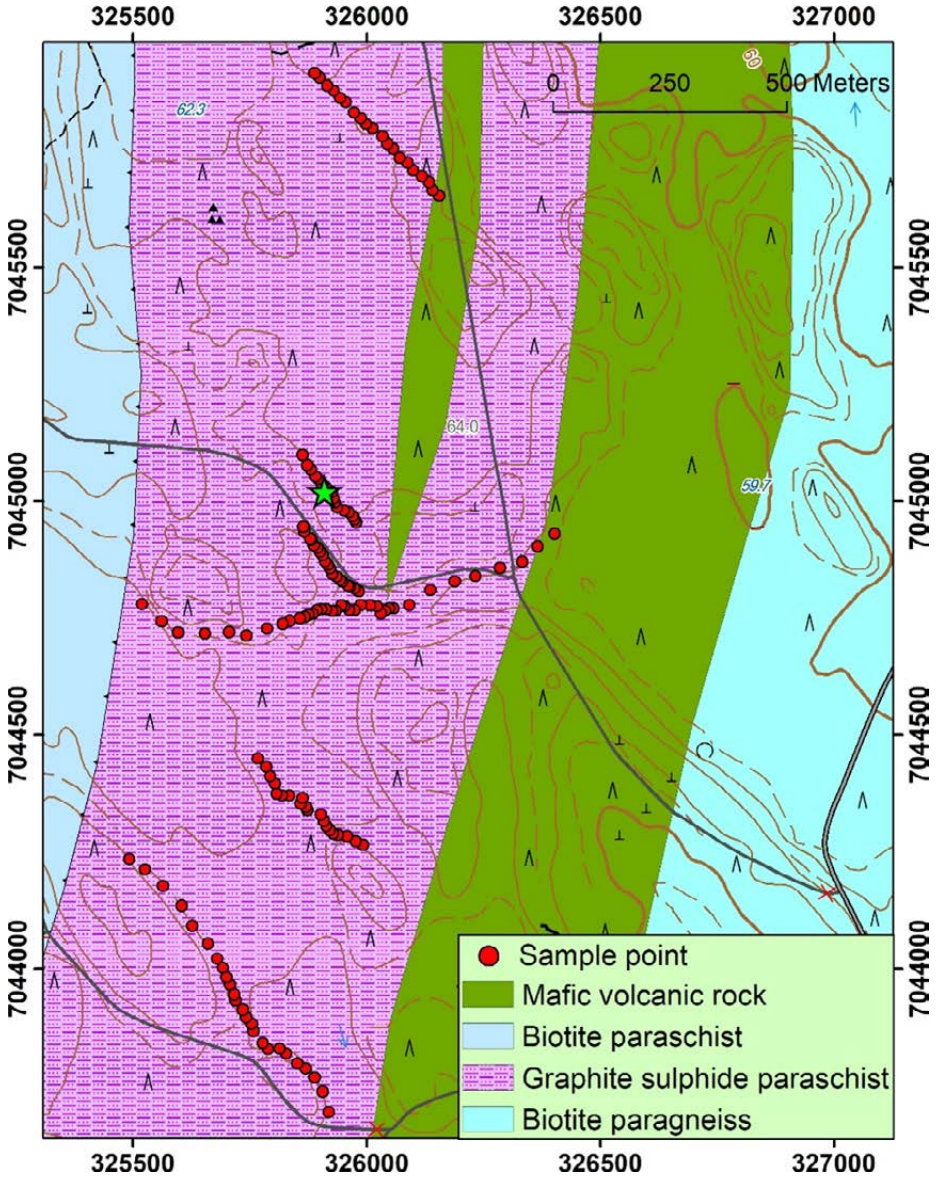

Fig. 22. The sample points on the bedrock map (Bedrock of Finland scale-free © Geological Survey of Finland 2022). The site of the mineralized drill core P4222019R7 is indicated with a green star. Basemaps © National Land Survey of Finland.

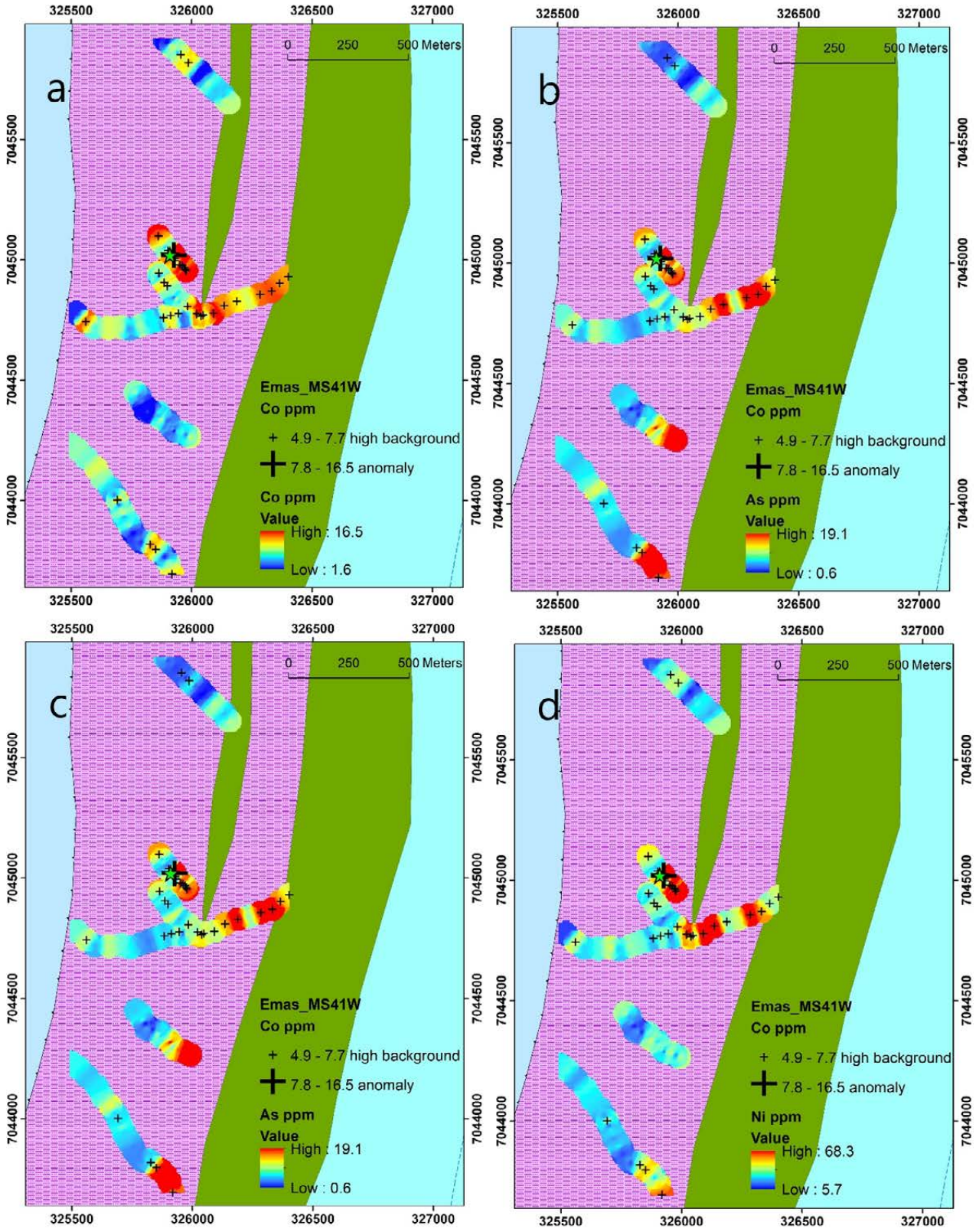

Fig. 23. a–d) The interpolated concentration of Co, As, Cu and Ni is presented on the bedrock map (Bedrock of Finland scale-free © Geological Survey of Finland 2022). The concentration of Co using a classification based on the Tukey boxplot is also displayed. Note that only the two highest classes of the Co concentration are presented. The site of drill core P4222019R7 is indicated with a green star.

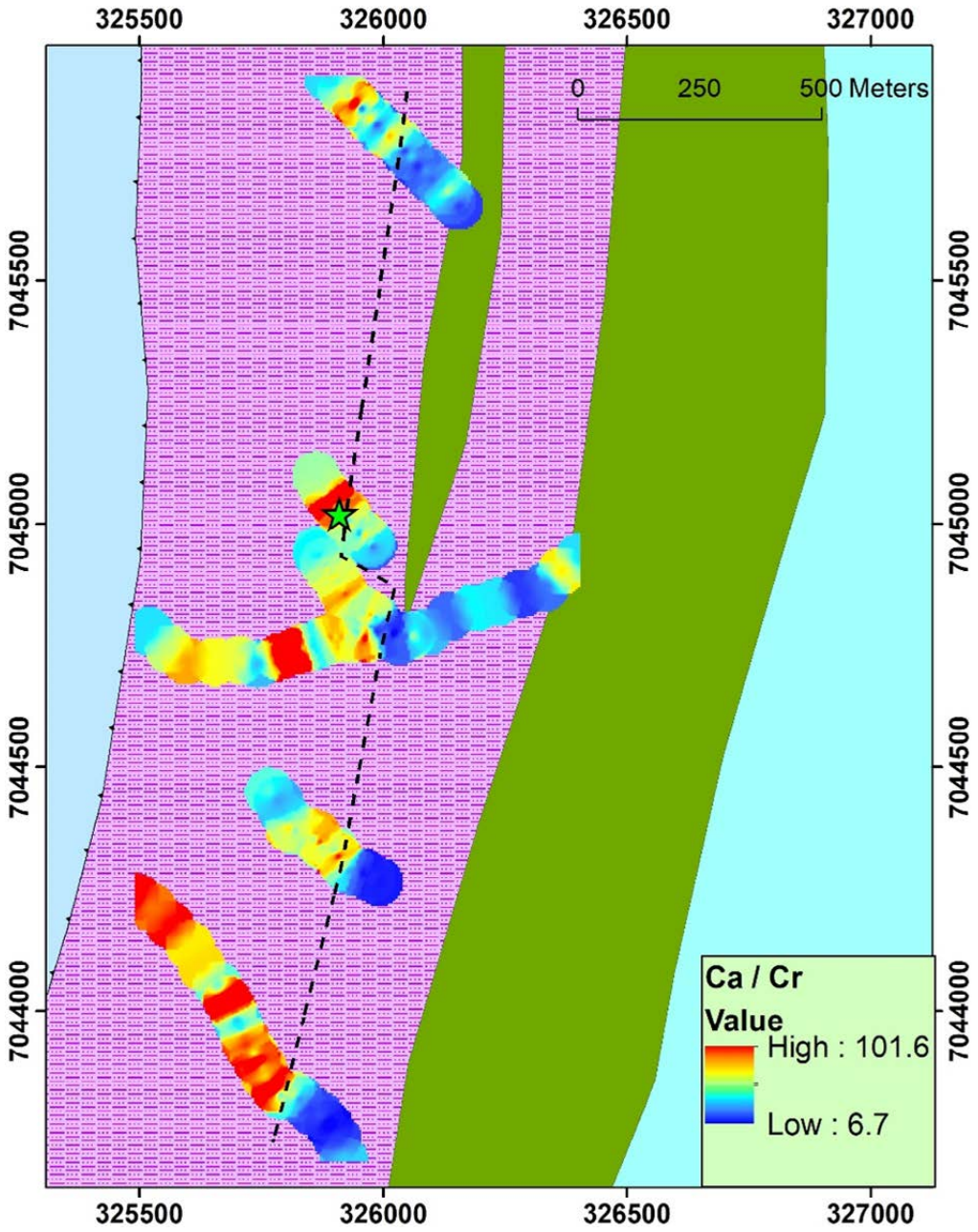

Fig. 24. The interpolated concentration of Ca/Cr is presented on the bedrock map (Bedrock of Finland scale-free © Geological Survey of Finland 2022). The site of drill core P4222019R7 is indicated with a green star. The mineralization is associated with the lithological contact zone, which is shown as a dashed line.

7 MINERALOGY

7.1 Materials and methods

A total of 20 polished thin sections were selected from 6 drill hole in the Emas area. The selected samples underwent mineralogical and micro-textural characterization by optical microscopy under transmitted and reflected light and SEM. Qualitative microanalysis of Ni–Co–As–Zn–Cu-bearing phases was conducted by using a Hitachi High-Tech SEM/EDS model SU3900, equipped with an X-ray detector for elemental analyses at the GTK mineral laboratory, Espoo, Finland. The modal content of Ni–Co–As–Zn–Cu-bearing phases, and associated pyrite and pyrrhotite, in the selected thin sections with a high sulphide content was measured using X-ray feature analysis, particle-by-particle and

point count scanning electron microscopy (SEM). The mineralogical studies on graphite are described in the beneficiation chapter.

Mineral chemistry data were derived for twelve thin sections at the Geological Survey of Finland on a CAMECA SX100 electron microprobe equipped with five wavelength-dispersion spectrometers (TAP, 2 LLIF, PET and LPET) and one EDS detector. The sulphide analyses were performed using an accelerating voltage of 20 kV and a probe current and beam diameter of 40 nA and 1 µm, respectively. Natural minerals and metals were used as reference standards. Data from the EPMA spot analyses are presented in Table 5.

The chemical analyses for the graphite-bearing rocks were carried out by Eurofins Labtium Oy. Major and minor elements were determined by using a combination of ICP-OES and ICP-Ms. Total carbon (TC) was determined with ELTRA analysers, while the whole rock and total sulphur (TS) contents were determined with ICP-MS technology. Representative analyses are listed in Table 6.

7.2 Sulphide occurrence and texture

The sulphide mineralization is hosted by sulphide and sulphide–graphite schists (black schists) and quartz–biotite–amphibol gneiss logged as amphibolite. The host rocks are moderately to strongly foliated, with some evidence of fold closures within the mineralized zones. The studied schist rocks are marked by an abundance of fine graphite (<30 µm to 200 µm in diameter) and commonly associated with sulphide minerals. Here, we delineate the microstructural characteristics of these minerals according to the different mineralization types, as illustrated in the backscattered electron images in Figure 25.

The main sulphide minerals in the Emas area are pyrite (FeS2), pyrrhotite (Fe1-xS), sphalerite (ZnS) and chalcopyrite (CuFeS2). Some nickel–arsenide–cobalt minerals occur as accessory phases, as represented by nickel–arsenide, including nickeline (NiAs), and sulpharsenides of nickel and cobalt, such as cobalt gersdorffite (NiAsS), cobalt pentlandite ((Fe,Ni)9S8) and cobaltite (CoAsS). Pyrite is seen to be present in a cubic form, a skeletal shape, as pyrite and pyrrhotite-forming breccia and anhedral elongated thread and/or subhedral crystals filling microfractures. However, chalcopyrite and sphalerite usually occur as subhedral to anhedral disseminated grains embedded in the silicate matrix and as inclusions in pyrite (Fig. 25a,b). In addition, galena is observed within sphalerite and chalcopyrite as filling cracks (Fig. 25b). Pentlandite is the most common nickel–iron sulphide containing a cobalt metal in the studied area, replaces pyrite and chalcopyrite (Fig. 25c) and occurs as small elongated grains (50–300 µm) within and/or at the rims of chalcopyrite (Fig. 25c). In addition, it fills interstices of corroded pyrite aggregates and fractures in pyrrhotite, indicating its later deposition in the ore stage. Nickeline occurs as small subhedral small grains, usually enclosed by pentlandite. Cobalt is distributed in the following mineralogical phases: cobaltite, gersdorffite, cobalt pentlandite, Co-rich arsenopyrite, pyrrhotite and pyrite. Cobaltite–gersdorffite crystals are present in nearly all the studied samples, with exceptionally large crystals that that high contents often appearing in sample R22. Cobaltite–gersdorffite mainly appears as euhedral crystals 100–1500 µm across within chalcopyrite and pyrite or interstitial to silicate minerals (Fig. 25d). Cobaltite, gersdorffite, Co-pentlandite show an extensive solid solution with respect to Co–Ni and As–S phases, which have intergrown with pyrite and chalcopyrite. In addition, cobaltite appears as euhedral crystals with sizes of 10–200 µm, and the crystals display relatively homogeneous characteristics under optical microscopy and scanning electron microscopy. Mapping of the elemental distribution of Co, Ni, As, Fe and S was performed, as shown in Figure 27. The contents of cobalt, nickel and arsenide display an obvious inverse correlation, while Fe and S are distributed uniformly, which might be attributed to the form of the cobaltite–gersdorffite solid solution or the varying degrees of pyrrhotite metasomatism (Han et al. 2020).

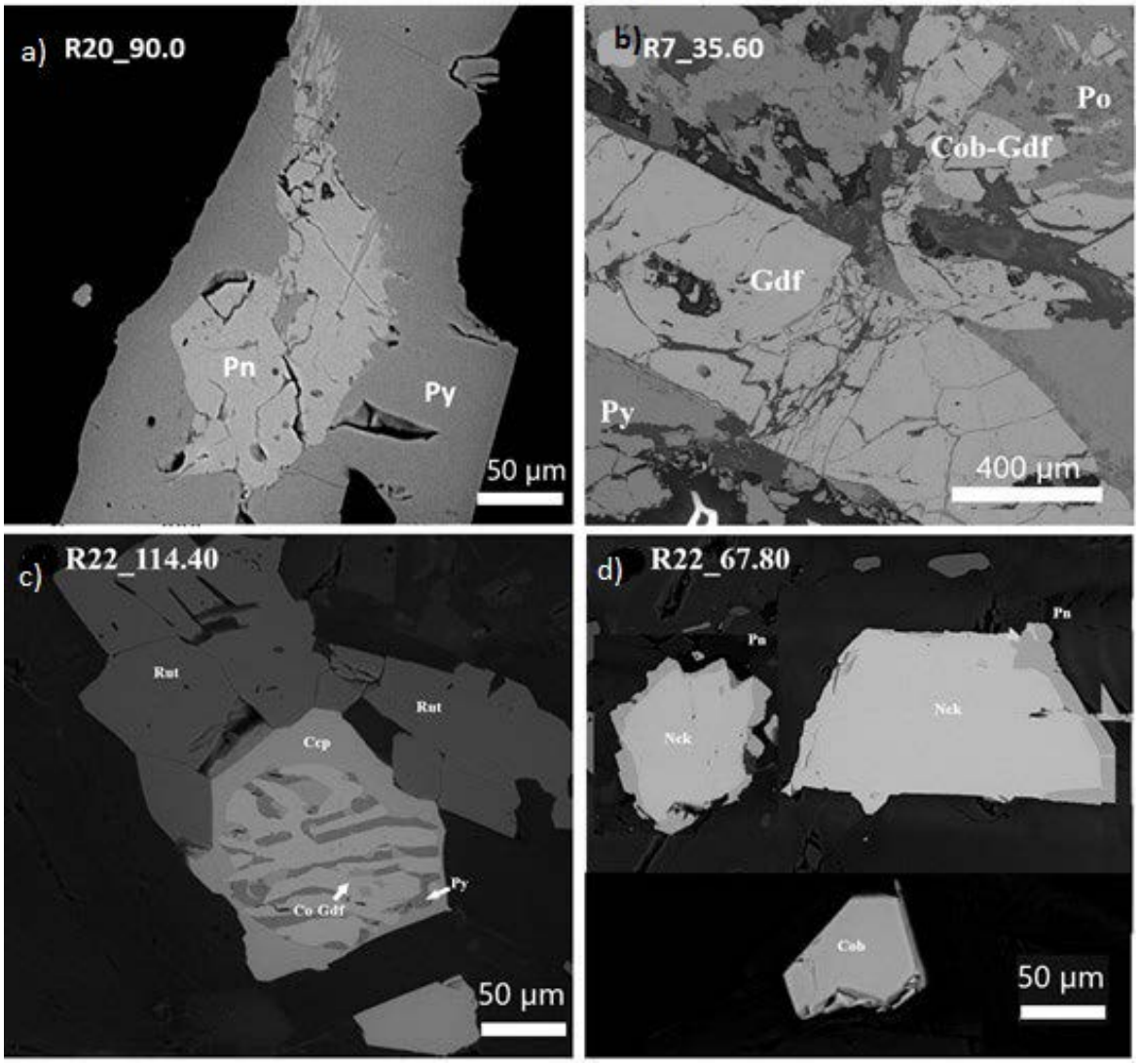

Fig. 25. A selection of backscattered electron microscopy images from the Emas sulphide phases. a) Cobalt pentlandite (Pn) with pyrite, b) cobaltite (Cob) and gersdorffite (Gdf) are present as large crystals, c) gersdorffite belongs to a solid solution series with cobaltite and d) nickeline (Nck) occurs as small subhedral small grains enclosed by pentlandite.

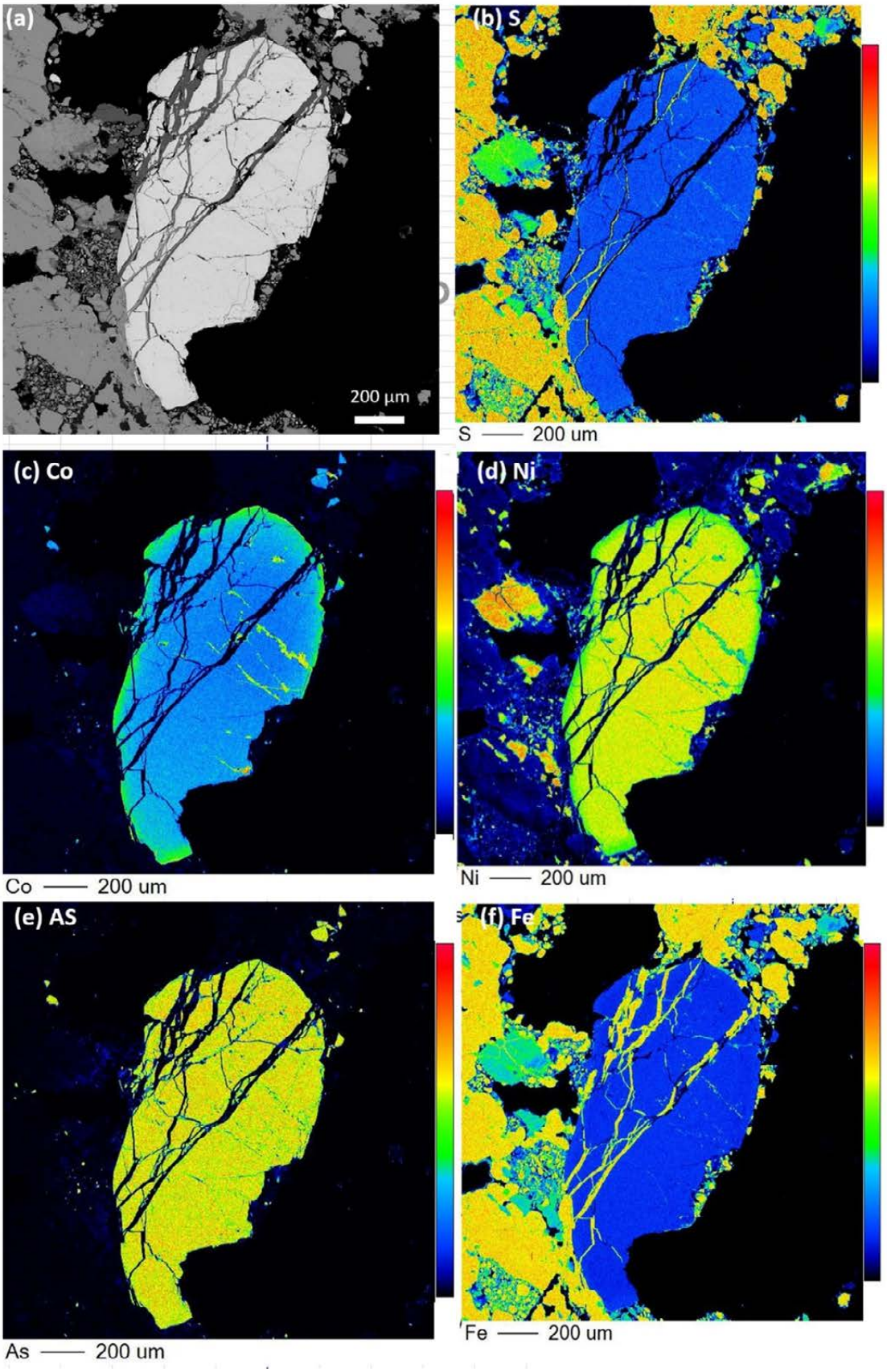

Fig. 26. Major element (Co, Ni, As, Fe and S) maps of a Co–gersdorffite crystal in sample R7_35.60.

7.3 Mineral chemistry of metal sulphides

Microprobe analysis revealed that cobalt is distributed in cobaltite, gersdorffite and pentlandite (Table 5). The cobaltite compositions are 18.6–21.7 wt% S, 13.6–17.5 wt% Co, 10.0–14.6 wt% Ni and 43.1–44.8 wt% As. Gersdorffite grains are composed of 15.7–23.4 wt% S, 5.3–12.9 wt% Co, 13.7–21.5 wt% Ni and 39.5–48.4 wt% As, while the pentlandite compositions are 28.2–36.4 wt% S, 22.0–30.9 wt% Fe, 26.6–34.9 wt% Ni and 0.2–2.3 wt% Co. Nickeline is mainly associated with pentlandite and gersdorffite, with compositions of 56.1–57.4 wt% As, 40.6–43.8 wt% Ni, 0.0–1.5 wt% Fe and 0.1–0.4 wt% Co. Sb-bearing niccolite nodules with thin crusts of gersdorffite–cobaltite and with late growth of euhedral ullmannite were observed in some samples. The ullmannite (NiSbS) compositions are 24.9–34.5 wt% S, 15.7–25.1 wt% Fe, 9.9–15.8 wt% Ni and 10.1–18.1 wt% Sb. The total zinc in sphalerite mainly occurs in association with pyrite and pyrrhotite. The sphalerite compositions are 34.4–55.4 wt% S, 0.0––2.4 wt%, Fe: 5.8-16.3 wt% and Zn: 37.0-56.6 wt%. The total copper is concentrated in chalcopyrite with composition of S: 32.7-34.7 wt%, Fe: 30.0-31.7 wt% and Cu: 32.9-34.3 wt%. EPMA analyses on the Co–Ni–As phases in the Emas are summarized in Figure 27. The diagrams display the chemical variability of the cobalt and nickel tend to enter cobaltite, gersdorffite and pentlandite phases, rather than existing in chalcopyrite and pyrrhotite. Almost all Co–Ni–As minerals are formed during through a hydrothermal process, which gathered nickel and cobalt elements widely (Han et al. 2020, Moroni et al. 2019). Sphalerite is an abundant sulfide mineral in the Raisjoki area, and it replaces pyrite, pyrrhotite and chalcopyrite. Electron microprobe analyses of sphalerite are in Table 5. Microprobe analyses revealed that the Fe content in the sphalerite ranges from 5.8 wt% to 16.3 wt%, S from 34.4 to 54.6 wt%, Mn from 0 to 2.4 wt% and Zn from 36.9 to 56.6 wt%. In addition, sphalerite records As, Ni, Sb and Cu contents above the limit of detection, probably related to sub-microinclusions of some sulphide phases.

Table 5. Summary of average EPMA data for Co–Ni–As–Zn sulphides (wt%).

Sample	Co	Fe	As	Zn	Ni	Sb	Cu	S	Te	Total
Cobaltite (CoAsS)										
R7_35.60 Gr2_1	16.30	7.88	44.75	0.00	11.42	0.07	0.01	19.66	0.04	100
R7_35.60 Gr2_2	14.86	8.29	43.93	0.01	11.94	0.06	0.00	19.47	0.06	99
R7_35.60 Gr5_ 1	14.73	8.83	44.16	0.00	11.89	0.09	0.00	19.81	0.03	100
R7_35.60 Gr5_ 2	13.69	8.23	44.22	0.01	12.43	0.06	0.01	19.27	0.05	98
R22_67.80 Gr1_1	13.62	8.52	43.37	0.03	12.78	0.04	0.01	21.71	0.06	100
R22_67.80 Gr1_3	17.48	8.15	43.1	0.00	10	0.04	0.00	21.27	0.08	100
R22_67.80 Gr1_4	17.02	6.72	43.1	0.00	14.61	0.05	0.01	18.55	0.07	100
Gersdorffite (NiAsS)										
R7_35.60 Gr1_1	11.75	8.64	45.15	0.00	14.92	0.08	0.00	19.12	0.06	100
R7_35.60 Gr1_2	10.19	8.41	45.91	0.00	16.33	0.07	0.00	18.78	0.03	100
R7_35.60 Gr2_1	10.66	8.48	45.35	0.00	16.00	0.07	0.00	18.42	0.05	99
R7_35.60 Gr2_2	11.29	8.55	45.62	0.00	15.48	0.07	0.00	19.00	0.04	100
R7_35.60 Gr3_1	11.48	8.86	45.28	0.00	14.46	0.06	0.00	19.09	0.03	99
R7_35.60 Gr3_2	10.52	8.90	45.34	0.00	15.84	0.06	0.00	18.68	0.05	99
Pentlandite $(Fe,Ni)_9S_8$										
R22_77.70 Gr1_1	2.25	29.90	0.00	0.00	34.32	0.00	0.00	33.14	0.06	100
R22_77.70 Gr1_2	2.30	29.96	0.00	0.00	34.20	0.00	0.00	32.99	0.06	100
R22_77.70 Gr6_1	2.12	29.90	0.03	0.00	33.99	0.00	0.00	33.14	0.08	99
R22_77.70 Gr6_2	2.07	29.57	0.00	0.00	33.01	0.00	0.00	31.67	0.07	96

Table 5. Cont.

Sample	Co	Fe	As	Zn	Ni	Sb	Cu	S	Te	Total
R22_77.70 Gr6_3	2.04	29.62	0.00	0.00	33.79	0.00	0.00	32.87	0.07	98
R22_77.25 Gr4_1	1.80	29.95	0.00	0.00	34.38	0.00	0.00	33.12	0.07	99
R22_77.25 Gr4_2	1.79	30.17	0.01	0.00	34.33	0.00	0.00	33.10	0.06	99
R22_77.25 Gr4_3	1.71	30.15	0.00	0.00	34.28	0.00	0.00	33.05	0.07	99
Nickeline NiAs										
R7_66.0_Gr1_1	0.06	0.00	56.08	0.03	43.56	0.00	0.00	0.02	0.04	100
R7_66.0_Gr1_2	0.11	0.01	56.70	0.00	43.83	0.00	0.00	0.02	0.00	101
R7_66.0_Gr1_3	0.09	0.00	56.89	0.00	43.48	0.00	0.00	0.03	0.00	100
R7_66.0_Gr2_1	0.39	0.00	56.82	0.00	41.42	0.04	0.00	0.38	0.00	99
R7_66.0_Gr2_2	0.32	0.01	57.35	0.00	42.21	0.00	0.00	0.00	0.00	100
R22_67.80_Gr1_1	0.06	0.00	56.91	0.00	43.1	0.04	0.00	0.02	0.00	100
R22_67.80_Gr1_2	0.11	0.01	56.52	0.00	43.49	0.05	0.00	0.02	0.00	100
R22_67.80_Gr1_3	0.09	1.52	56.21	0.00	40.56	1.71	0.00	0.03	0.00	100
Sphalerite ((Zn,Fe)S										
R20_77.8_Gr7	0.03	7.9	0.00	40.79	0.00	0.04	0.04	0.56	51.24	101
Chalcopyrite ($CuFeS_2$)										
R22_77.25 Gr1	0.00	31.53	0.03	0.00	0.05	0.00	34.01	34.48	0.02	100
R22_77.25 Gr3	0.00	31.69	0.01	0.00	0.02	0.00	33.91	34.67	0.00	100
R22_77.25 Gr4	0.00	31.51	0.00	0.00	0.03	0.00	34.11	34.63	0.00	100
R22_77.25 Gr5	0.00	29.99	0.01	0.00	0.15	0.00	32.89	32.70	0.00	96
R22_77.25 Gr6	0.00	31.37	0.00	0.00	0.06	0.00	34.30	34.36	0.00	100

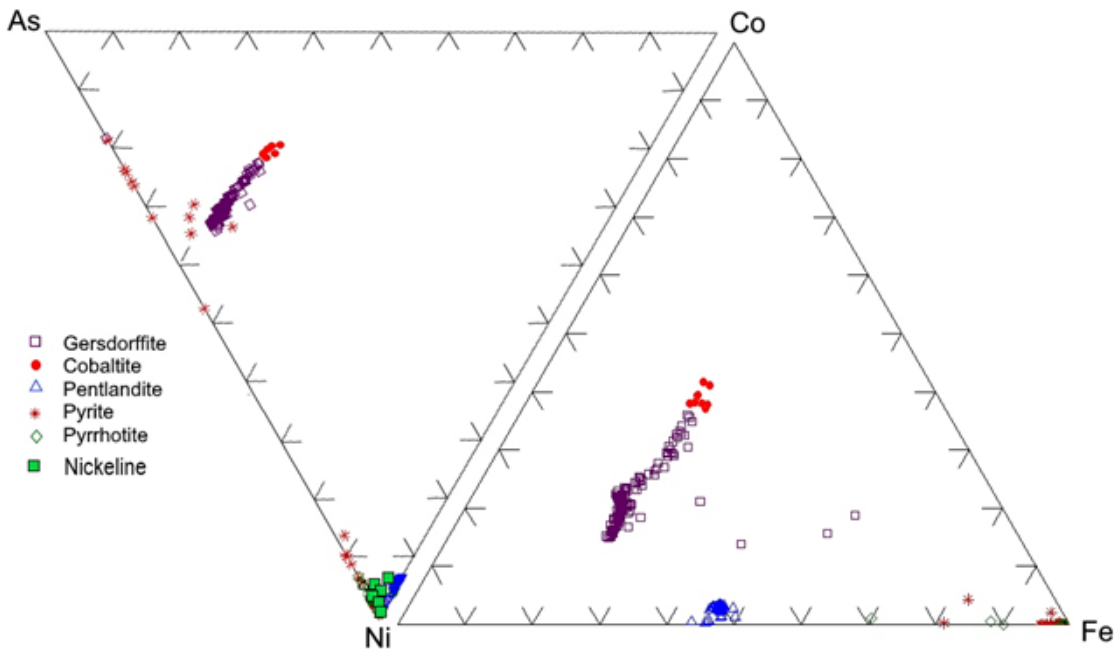

Fig. 27. Ternary diagrams comparing polymetallic Ni–Co–As and Fe phases.

Uraninite as discrete disseminated grains was detected in some samples, but are quite rare. (Fig. 28). The uraninite grains are usually rounded to subhedral in shape, and only rarely are euhedral varieties observed; the uraninite grains occur either at the rims of apatite crystals or in very thin fissures associated with bastnasite and xenotime or as inclusions within pyrite. Semi-quantitative electron microprobe analyses of the uraninite yielded an average composition of 69.5 wt% UO_2, 17.8 wt% PbO, 5.4 wt% SiO_2 and 7.1 wt% FeO. The correlation of U with Pb is linear and positive, which is due to radiogenic lead being a product of the radioactive decay of uranium (Fig. 8f). Moreover, small amounts of titanium, yttrium and thorium were introduced with the uranium and are probably incorporated in the uraninite lattice.

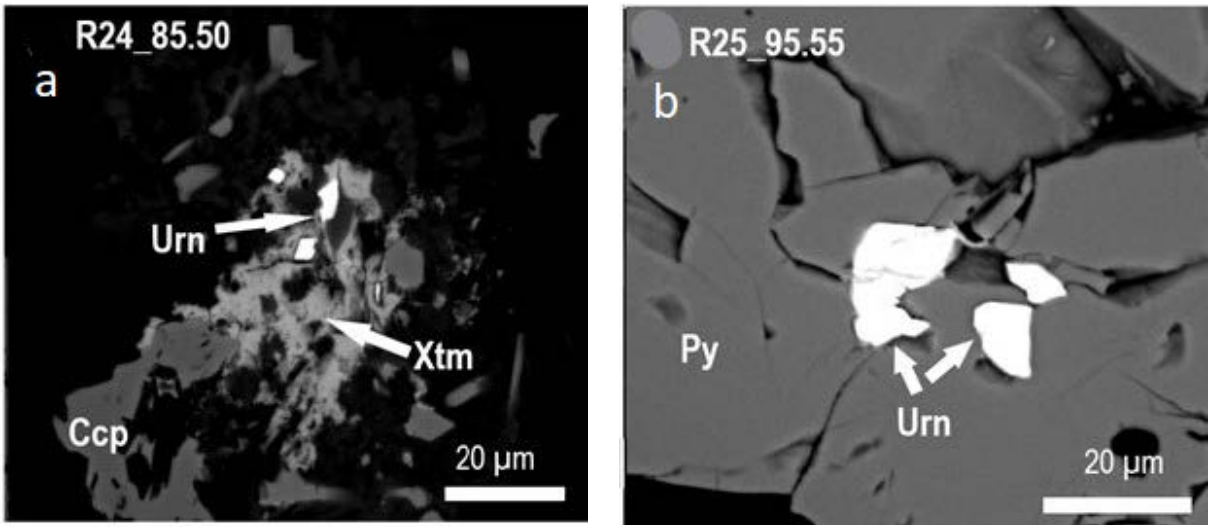

Fig. 28. a) and b) A selection of backscattered electron microscopy images of uraninite as discrete disseminated grains from the Emas samples.

7.4 Modal mineralogy

SEM-EDS feature analysis was used to provide quantitative measurements of sulphide mineral abundances in selected samples, as illustrated in Figures 29 and 30. The feature analysis data document the enrichment factors (% mineral, as given in histograms) and modal abundances of the studied samples.

A total of 2204 mineral grains were analysed from a thin section of sample R7_35.60. The absolute abundances of the sulphide minerals were 65.3% gersdorffite, 26.4% Co-arsenopyrite, 4.8% cobaltite, 1.8% pentlandite and 1.6% pyrite, while nickeline (~68%) was the most abundant sulphide in sample R7_56.55 (Fig. 29).

A total of 1365 mineral grains were analysed in a thin section of sample R20_77.80. The absolute abundances of the sulphide minerals were 33% pyrite, 27.4% pyrrhotite, 16.3% sphalerite, 13.2% chalcopyrite, 8.4% ilmenite, 1.1% pentlandite, 0.4% gersdorffite and 0.3% uraninite (Fig. 30).

R7_35.60

Mineral	Mineral	Point count	Mineral %
Gersdorffite (Gdf)	Gdf	1440	65.3
Co-Arsenopyrite (Apy)	Apy	582	26.4
Cobaltite (Cob)	Cob	106	4.8
Pentlandite (Pn)	Pn	40	1.8
Pyrite (Py)	Py	36	1.6
Total		2204	

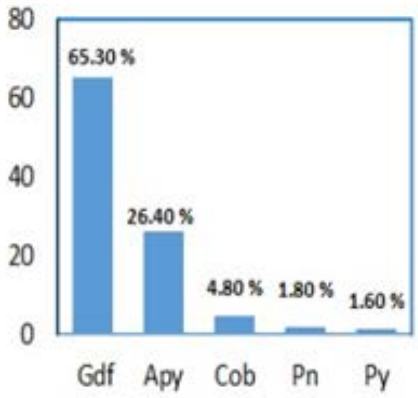

R7_56.55

Mineral		Point count	Mineral %
Nickeline (Nck)	Nck	150	68.2
Gersdorffite (Gdf)	Gdf	50	22.7
Cobaltite (Cob)	Cob	15	6.8
Ilmenite (Ilm)	Ilm	5	2.3
		220	

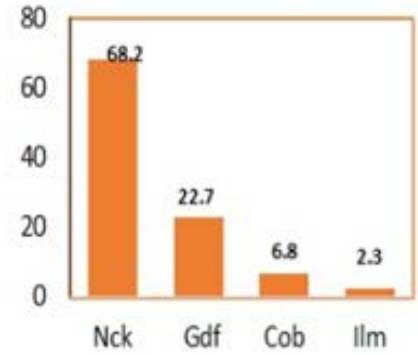

R7_66.0

Mineral		Point count	Mineral %
Pyrite (Py)	Py	644	42.1
Pyrrhotite (Po)	Po	345	22.5
Chalcopyrite (Ccp)	Ccp	232	15.2
Pentlandite (Pn)	Pn	130	8.5
Ilmenite (Ilm)	Ilm	75	4.9
Gersdorffite (Gdf)	Gdf	52	3.4
Co-Arsenopyrite (Apy)	Apy	22	1.4
Cobaltite (Cob)	Cob	18	1.2
Sphalerite (Sp)	Sp	12	0.8
		1530	

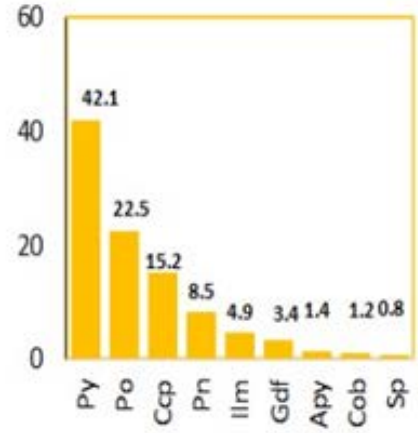

R7_68.60

Mineral		Point count	Mineral %
Pyrite (Py)	Py	750	42.5
Pyrrhotite (Po)	Po	454	25.7
Chalcopyrite (Ccp)	Ccp	220	12.5
Pentlandite (Pn)	Pn	175	9.9
Ilmenite (Ilm)	Ilm	105	5.9
Gersdorffite (Gdf)	Gdf	35	2.0
Sphalerite (Sp)	Sp	26	1.5
		1765	

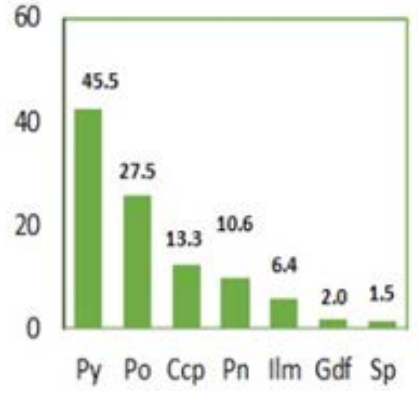

Fig. 29. Modal mineralogy of sulphides determined by X-ray feature analysis, particle-by-particle and point count scanning electron microscopy for some samples from drill hole R7.

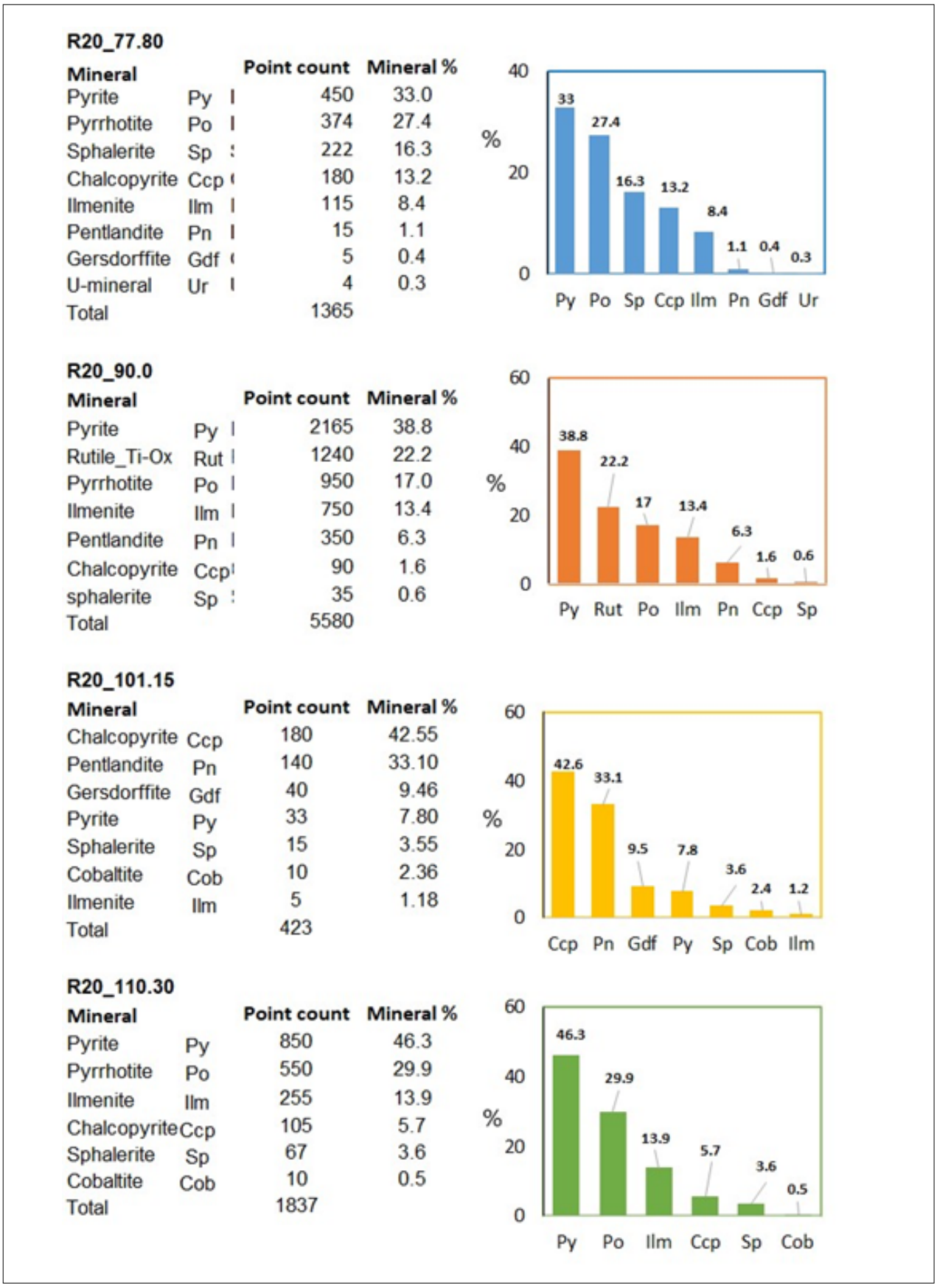

Fig. 30. Modal mineralogy of sulphides determined by X-ray feature analysis, particle-by-particle and point count scanning electron microscopy for some samples from drill hole R20.

7.5 Geochemical characteristics of sulphides

The Al–(Fe + Ti)–Mg classification diagram (Jensen 1976) indicates that most of the studied samples cluster on the border of high-Fe (HFT) and high-Mg (HMT) tholeiitic basalt. Some of the samples are Mg rich and plot in the basaltic komatiitic (BK) field.

Table 6. Selected samples with a high content of metal sulphides from the Emas area.

Sample	Co	As	Ni	Cu	Zn	S wt%	C wt%
R7 32.50-33.70	910	3800	8800	519	162	7.57	1.01
R7 33.70-34.70	4820	18 400	29 700	611	103	22.9	1.03
R7 34.70-35.35	5310	18 700	15 700	3470	147	14.1	0.32
R7 35.35-35.85	8510	44 900	40 100	431	121	26.5	0.27
R7 35.85-36.50	515	2520	5240	257	189	4.5	0.11
R7 36.50-37.0	173	332	2540	199	200	2.39	0.61
R7 37.00-38.0	202	61	3480	170	235	3.63	0.19
R7 38.00-39.0	298	21	6340	371	277	6.49	0.13
R7 39.00-40.0	301	66	4030	178	313	2.58	0.07
R7 40.00-41.0	259	31	3310	383	208	3.57	0.09
R22 67.00-68.0	297	1630	2410	188	134	1.4	
R22 68.00-69.0	173	110	2320	159	188	1.07	
R22 69.00-70.0	357	1200	2550	382	157	1.31	
R22 77.00-78.0	440	31.4	7510	287	148	6.77	
R22 78.00-79.0	205	75.4	2090	258	195	1.24	
R23 99.0-100.0	134	62.7	1950	134	163	0.801	
R23 100.0-101.0	152	250	2480	163	162	1.23	
R24 85.0-86.0	249	10.2	4830	320	178	6.67	
R24 86.0-87.0	105	5.75	1680	218	231	3.85	
R25 36.0-37.0	188	166	2090	131	177	1.11	
R25 37.0-38.0	186	95	1770	191	159	0.703	
R22 69.0-70.0	357	1200	2550	382	157	1.31	
R22 77.0-78.0	440	31.4	7510	287	148	0.587	
R24 78.0-79.0	298	52.5	1570	287	104	0.59	

Table 7. Selected samples with a high content of U and metal sulphides from the Emas area.

Sample	U	As	Co	Cu	Ni	Zn	S %	C *
R7 113.0-114.0	27.2	1.84	24.2	295	316	1180	4.29	
R22 38.0-39.0	35.1	5.33	72.9	120	490	450	4.22	1.11
R24 66.0-67.0	28.4	27.8	19.8	379	280	591	3.96	9.46
R24 67.0-68.0	35.6	30.7	37.2	397	400	1090	5.7	12.6

*Accredited analysis with carbon analyser

The relations between Ni, Co, As and Zn versus sulphur and carbon can be observed from Table 4, which indicates that base metals are incorporated into sulphide mineralization types (i.e., pyrrhotite and pyrite-dominant types). According to the results, Ni, As and Co indicate a strong inter-metallic correlation, which can be attributed to the common metal-bearing mineral association of gersdorffite (NiAsS), pentlandite ($(Fe,Ni)_9S_8$), nickeline (NiAs) and cobaltite (CoAsS) in the studied samples (Table 4). Mostly in black schist sections (drill hole R7), Zn locally attains concentrations between 400 and 2420 ppm.

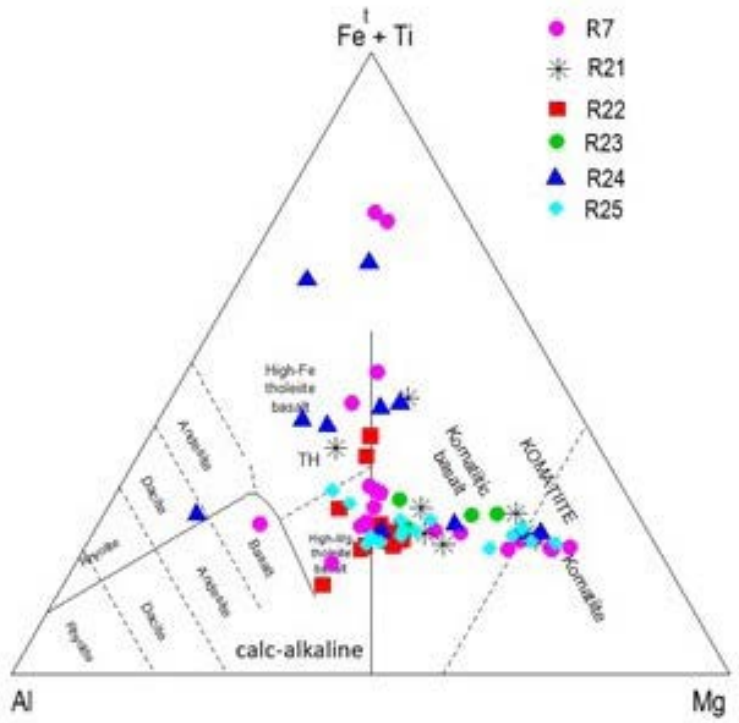

Fig. 31. Jensen's cation plot for sulphide-rich samples from the Emas area (after Jensen 1976).

8 BENCH-SCALE TEST OF EMAS GRAPHITE

Beneficiation studies were conducted with samples from the Emas graphite occurrence in January 2021. The previous tests were performed in October 2020 using a rod mill and ball mill in the grinding procedure, which resulted after flotation in a C concentrate below 50%. In the second test, a new procedure was developed aiming to increase the C grades and recoveries of the graphite concentrate through ultrafine grinding with an attritor mill.

8.1 Materials and sample preparation

Before the samples were sent for beneficiation at Mintec Outokumpu, the quality of the graphite was mineralogically assessed by petrographic analysis under an optical microscope. Similar studies were done for the neighbouring Raisjoki belt black schists (Al-Ani et al. 2020, Kuusela et al. 2020). The study indicated that the sample primarily consists of quartz, alkaline feldspar and biotite with subordinate graphite, pyrite, carbonate and chlorite.

Most of the graphite flakes occurred as small, flat, plate-like crystals (30 to 200 µm). In some samples, the graphitic schists can be rich in pyrrhotite, which is relatively easily deformed. This schist texture shows crystals of graphite "float" in a matrix of pyrrhotite (Fig. 2c). Altogether, 16 kg of drill cores was received from Emas. The drill core samples were crushed to 100% -1.6 mm and homogenized and split into 1-kg and 5-kg samples. The samples were prepared during the first part of the project in January.

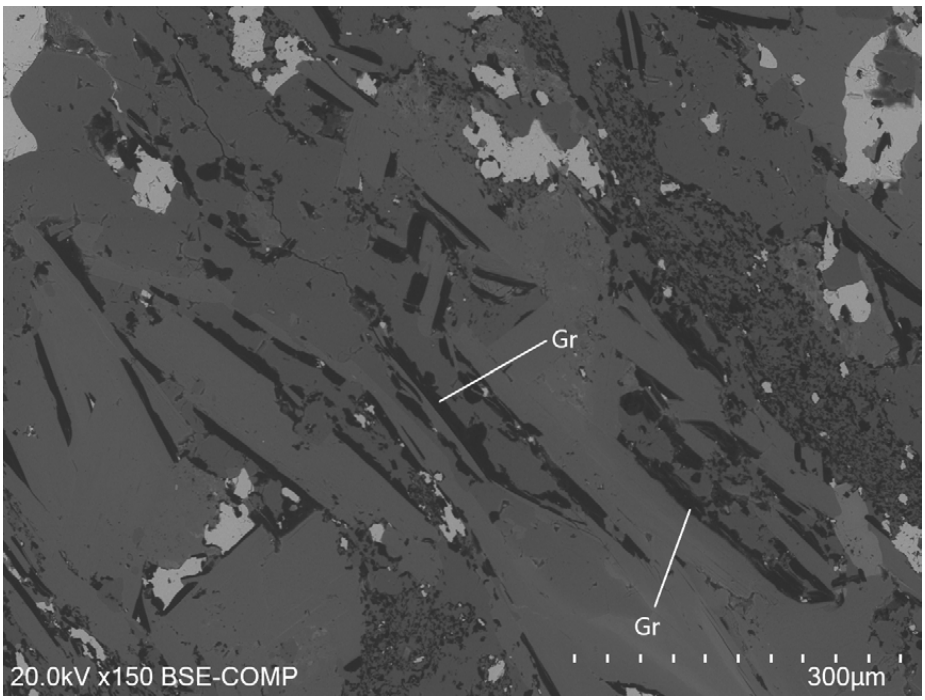

Fig. 32. A SEM image of Emas black schist. Gr = graphite.

8.2 Analytical methods

Chemical analyses of process products were carried out by Eurofins Labtium Oy/CRS Laboratories Oy, located in the same premises as GTK Mintec in Outokumpu. The chemical analytical methods were X-ray fluorescence (XRF) for the main elements and Eltra or Leco for C.

8.3 Methods of test work

The crushed samples were used for bench-scale flotation tests. In total, two tests were carried out for the sample. The main difference compared with the previous test was the implementation of ultrafine grinding by using a stirred media mill. A magnetic separation stage was added in some tests after the first grinding. Graphite was concentrated by froth flotation with a rougher stage. Regrinding of the rougher concentrate was tested. The rougher concentrate was cleaned in three to four cleaning stages. The final graphite cleaner concentrate was purified by alkaline roasting and acid leaching.

8.4 Flotation

Different flotation tests were performed to obtain information about the sample behaviour in flotation and optimize the conditions, seeking high C grades and recoveries for each test performed. Three different tests were carried out, of which the first stage of the flotation tests was grinding with a rod mill. The inner dimensions of the mill were Ø190 × 220 mm and it was charged with 8.0 kg of Fe rods. Grinding was performed wet, using tap water (0.9 L) at room temperature. The grinding time was 75 minutes.

Ultrafine grinding was performed using a Union Process Attritor, Model 1S. It was used with 3- to 4-mm-diameter ceramic balls, 564 rpm, 3.8 L balls and approximately 20% solids.

Wet magnetic separation was carried out using a SALA magnetic separator at 0.3 T. The non-magnetic fraction was directed to froth flotation. Flotation experiments were performed in an Outokumpu-type flotation machine (No. 3) in 2.5- or 4-litre flotation cells. In all tests, kerosene and MIBC were used. The kerosene dosage

was 400–300 g/t in the tests, and the MIBC dosage was 100–150 g/t. The tests continued with a rougher stage and four cleaners (Fig. 35). The rougher concentrate in E-T07 was reground with the attritor mill for 120 minutes. Figures 33 and 35 illustrate the different flowsheets tested during the test work.

Emas	E-T06	AM - 120 min	0.3 T	-	300	150	4
	E-T07	RM - 75 min	-	AM - 120 min	300	150	4

Fig. 33. Scheme of the stages in the flotation process. AM = attritor mill, RM = rod mill.

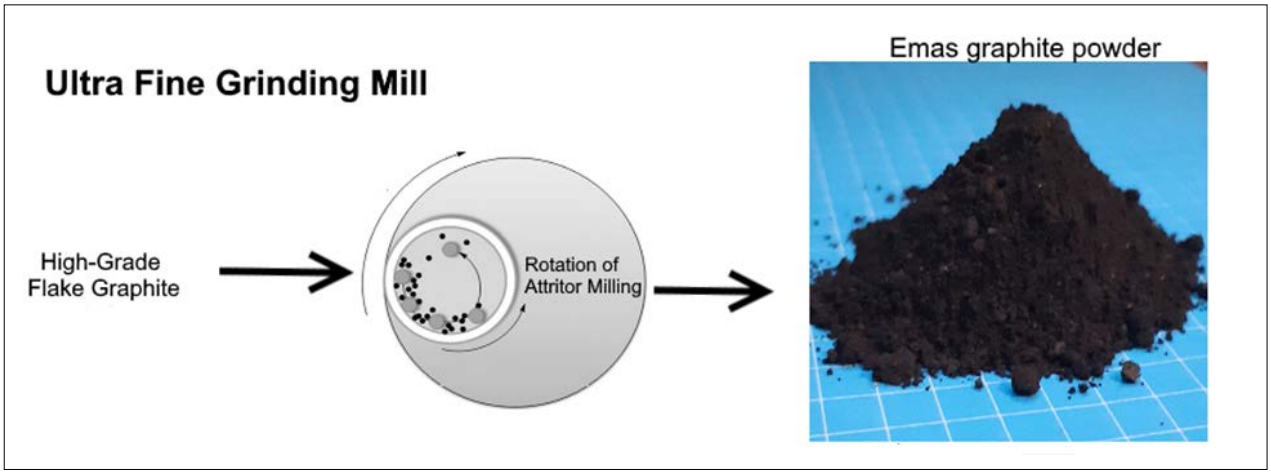

Fig. 34. Ultrafine grinding had a major impact on the outcome of the Emas beneficiation process.

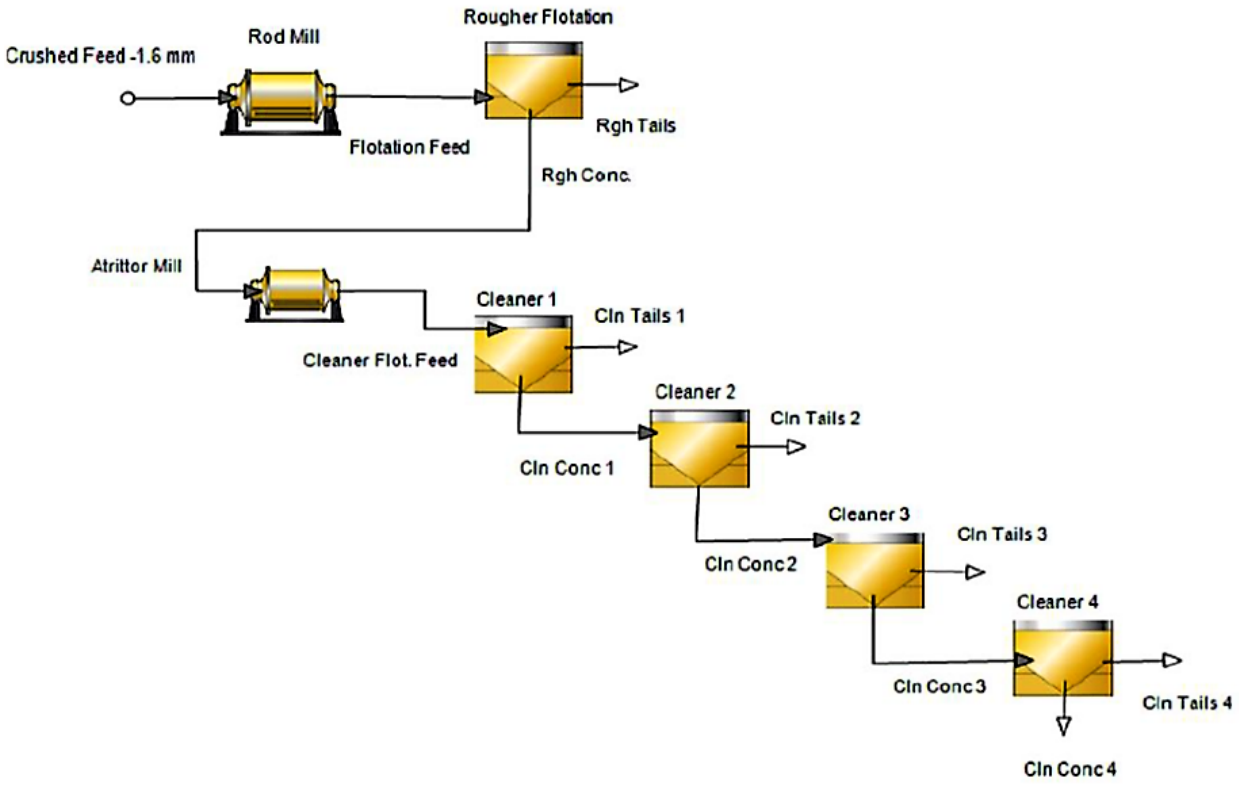

Fig. 35. Scheme of the E-T07 sample flotation stages that proved to be the most successful for Emas graphite beneficiation.

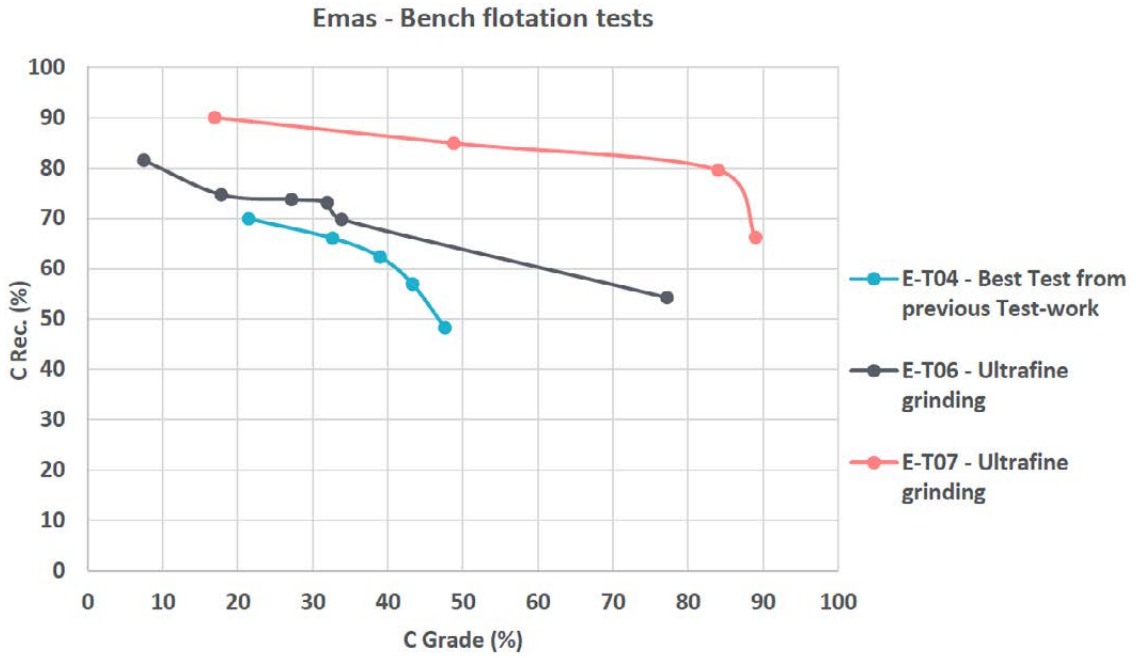

Fig. 36. The addition of ultrafine grinding with an attritor mill for Emas test samples E-T06 and especially ET07 significantly raised the C recovery grade and the C purity grade.

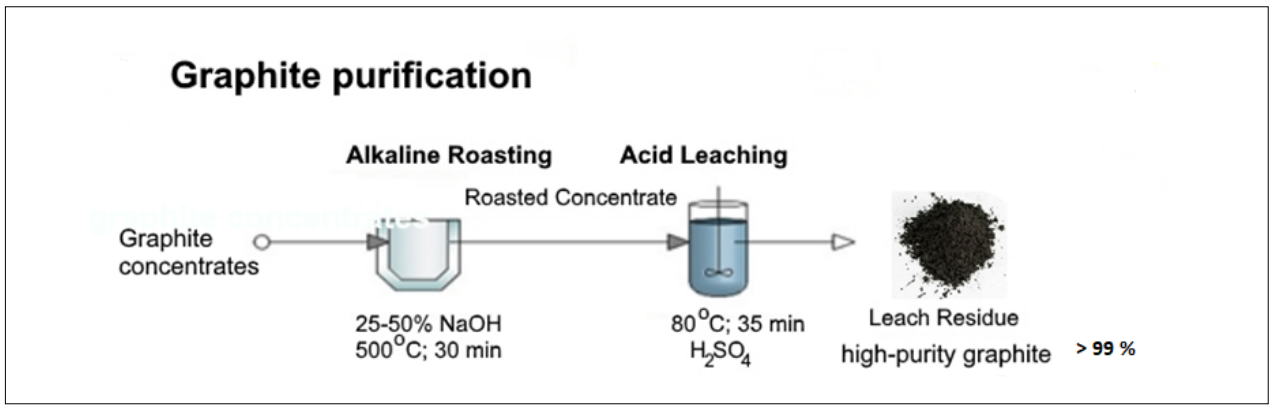

Fig. 37. Graphite purification test stages.

8.5 Floatation and purification results

The implementation of ultrafine grinding in the grinding procedure resulted in a considerable improvement in the third cleaner concentrate C grade for Emas compared to the previous test work. The Emas sample reached a C concentration of 87–89% with a recovery of 66% (Fig. 36).

For the purification test, the C grade of the Emas feed material was 86.9%. The final leached residue presented a C content higher than 99%. Although the C grade measured in the E-PT3 residue was 100%, the XRF indicated the presence of impurities. The highest impurity measured in the residue was 0.5% SiO_2 in the Emas sample. A different C analysis method should be applied for the leaching residue.

9 CONCLUDING REMARKS

Emas flake graphite is found in the Aho metavolcanic belt and is one of several volcanic sequences extending tens of kilometres in length and cutting the Ostrobothnian schist belt. GTK investigated the metavolcanic sequences in central and southern Ostrobothnia during 2019 to 2021 with the aim of mapping the battery mineral (Li–Ni–Co) potential. The volcanic sequences are clearly visible in conventional geophysical maps, mainly due to the high graphite content in black schists.

The Emas flake graphite mineralization, with flakes measured at 30–200 µm, was found in an exceptionally low-grade metamorphic terrain. Several of the flake graphite layers in 7–15 m intersections have an average graphitic carbon (Cg) content of over 7%.

GTK discovered a Ni–Co–Au-rich mineralization that is in close contact to a distinct rock type with ultramafic characteristics and has a strong Cr alteration signal that is also traceable in the surface. The main ore-forming minerals containing Ni–Co–Au were identified as gersdorffite, Co-aresenopyrite, cobaltite and pentlandite. The Ni–Co mineralized rock types are flanked on both sides by flake graphite-bearing black schists.

Based on two small diamond drilling programmes totalling 1152 m, the Ni–Co–Au mineralization contains at best 3 m @ 0.5% Co and 2% Ni with 2 m 0.32 ppm Au and has a weakened but open continuation to the N and S with layers of 15 or more metres in thickness containing 100–200 ppm Co and 0.1–0.2% Ni. The highest concentrations were recorded within rocks that had undergone extensive shear deformation, suggesting structural control of the mineralization. Lateral fault slip movement is also supported by a 144-sample surface geochemical sampling programme demonstrating sharp contact horizons with a high contrast in interpolated Ca/Cr values.

Before diamond drilling and after the drilling operations, geophysical ground measurements, including magnetic, multi-frequency EM and gravimetric measurements, were conducted to direct the drilling.

Beneficiation tests performed by Mintec Outokumpu were optimized for Emas flake graphite using ultrafine grinding in the floatation process, which gave an outcome of 89% purity and 66% recovery. After the purification process, a purity grade of >99% was achieved.

When the graphite content exceeds 4% Cg in Emas black schists, it has a good correlation with U and Zn. Radiometric maps may be an efficient aid to estimate the graphite content from a geophysical conductivity map.

The investigations indicate that the black schists in the volcanic sequences commonly associated with spodumene pegmatites have a good potential for flake graphite, a potential that may be applied to the whole region. Structures visible from geophysical signals, such as gravity signals and surficial Cr anomalies from soil samples within or in close proximity to black shists, could also serve as pathfinders for Ni–Co–Au mineralizations.

REFERENCES

Ahtola, T., Kuusela, J., Käpyaho, A. & Kontoniemi, O. 2015. Overview of lithium pegmatite exploration in the Kaustinen area in 2003–2012. Geological Survey of Finland, Report of Investigation 220. 28 p. Available at: https://tupa.gtk.fi/julkaisu/tutkimusraportti/tr_220.pdf

Al-Ani, T., Kuusela, J. & Nygård, H. 2020. Mineralogical Characterisation of Graphite Deposits in the Raisjoki area, Western Finland. Geological Survey of Finland, Open File Work Report 55/2020. 50 p. Available at: https://tupa.gtk.fi/raportti/arkisto/55_2020.pdf

Bedrock of Finland – DigiKP. Digital map database [Electronic resource]. Espoo: Geological Survey of Finland [referred 1.6 2021]. Version 2.1.

Carranza, E. J. M. 2009. Geochemical Anomaly and Mineral Prospectivity Mapping in GIS. Amsterdam: Elsevier. 368 p.

Han, Y., Liu, Y. & Li, W. 2020. Mineralogy of Nickel and Cobalt Minerals in Xiarihamu Nickel–Cobalt Deposit, East Kunlun Orogen, China. Frontiers in Earth Science 8, p. 597469. Available at: https://doi.org/10.3389/feart.2020.597469

Hautaniemi, H., Kurimo, M., Multala, J., Leväniemi, H. & Vironmäki, J. 2005. The 'three in one' aerogeophysical concept of GTK in 2004. In: Airo, M.-L. (ed.) Aerogeophysics in Finland 1972–2004: Methods, System Characteristics and Applications. Geological Survey of Finland, Special Paper 39, 21–74. Available at: https://tupa.gtk.fi/julkaisu/specialpaper/sp_039_pages_021_074.pdf

Hulkki, H. 2022. Akkumineraalipotentiaalin kartoitusprojektin Raisjoen tutkimusalueen vuosien 2019–2021 moreeninäytteenottojen tulokset. Geological Survey of Finland, Open File Work Report 7/2022. (in Finnish). (in prep)

Jensen, L. S. 1976. A new cation plot for classifying sub-alkaline volcanic rocks. Ontario Division Mines Miscellaneous Paper No. 66.

Kuusela, J., Ahtola, T., Koistinen, E., Seppänen, H., Hatakka, T. & Lohva, J. 2011. Report of investigations on the Rapasaaret lithium pegmatite deposit in Kaustinen–Kokkola, Western Finland. Geological Survey of Finland, archive report 42/2011. 29 p., 21 app. pages. Available at: https://tupa.gtk.fi/raportti/arkisto/42_2011.pdf

Kuusela, J., Nygård, H., Leväniemi, H. & Al-Ani, T. 2020. The investigations of the Raisjoki metavolcanic rocks in Evijärvi, Western Finland. Geological Survey of Finland, Open File Work Report 57/2020. 14 p., 2 app. pages. Available at: https://tupa.gtk.fi/raportti/arkisto/57_2020.pdf

Lehto, T. 2021. Structural control of dykes and veins in the Mansikka-aho area, Evijärvi, Western Finland. Master Thesis, University of Turku, Department of Geography and Geology. 52 p., 4 app. pages.

Lindmark, B. 1978. Raisjoen mustaliuskevyöhyke. Geological Survey of Finland, archive report M19/2314/78/1/10. 15 p. (in Finnish). Available at: https://tupa.gtk.fi/raportti/arkisto/m19_2314_78_1_10.pdf

Lindmark, B. 1979. Geologisen tutkimuslaitoksen malmitutkimukset Kaustisen Ahvenjärvellä vuosina 1970–1978. Geological Survey of Finland, archive report M19/2323/79/2/10. 27 p., 2 app. pages. (in Finnish). Available at: https://tupa.gtk.fi/raportti/arkisto/m19_2323_79_2_10.pdf

Lonka, A. 1981. Eräistä hiilipitoisista liuskeista Kaustisen kallioperäkarttalehdellä. Geological Survey of Finland, archive report M 19/2323/-81/1/81. 4 p., 18 app. pages. (in Finnish). Available at: https://tupa.gtk.fi/raportti/arkisto/m19_2323_81_1_81.pdf

Moroni, M., Rossetti, P., Naitza, S., Magnani, L., Ruggieri, G., Aquino, A., Tartarotti, P., Franklin, A., Ferrari, E., Castelli, D. & Oggiano, G. 2019. Factors controlling hydrothermal nickel and cobalt mineralization – Some suggestions from historical ore deposits in Italy. Minerals 9(7), p. 429. Available at: https://www.mdpi.com/2075-163X/9/7/429

Nygård, H., Kuusela, J., Leväniemi, H. & Kujasalo, J.-P. 2021. The investigation of the Kaitåsen metavolcanic rocks in Kruunupyy, Western Finland. Geological Survey of Finland, Open File Work Report 69/2021. 20 p. Available at: https://tupa.gtk.fi/raportti/arkisto/69_2021.pdf

Pearce, J. A. 1996. A User's Guide to Basalt Discrimination Diagrams. In: Wyman, D. A. (ed.) Trace Element Geochemistry of Volcanic Rocks: Applications for Massive Sulphide Exploration. Geological Association of Canada, Short Course Notes, Vol. 12, 79–113.

Ruskeeniemi, K. 1988. Mustaliuskeiden metallipitoisuuksista Kaustisen ja Evijärven karttalethtien alueella. Geological Survey of Finland, archive report M19/2314/88/2/30. 7 p., 2 app. pages. (in Finnish). Available at: https://tupa.gtk.fi/raportti/arkisto/m19_2314_88_2_30.pdf

Ruskeeniemi, K. 1991. Suomen proterotsooisten mustaliuskeiden uraanipitoisuudesta. Geological Survey of Finland, archive report M19/3344/91/1/30. 2 p., 15 app. pages. (in Finnish). Available at: https://tupa.gtk.fi/raportti/arkisto/m19_2314_88_2_30.pdf

Säynäjärvi, K. 1973. Kaivoslain 19 §:n mukaiset tutkimusselostukset valtausalueilla Ruokojärvi 1 ja Vinturi 1 suoritetuista töistä ja niiden tuloksista. Ministry of Trade and industry, claim report 1941/1. 3 p., 11 app. pages. (in Finnish). Available at: https://tupa.gtk.fi/raportti/valtaus/1941_1.pdf

Sipilä, E. 1989. Lito- ja pedogeokemiallinen tutkimus kesäkuussa 1979 Raisjoen Cu-Co-Ni-anomaalisten kansannäytteiden johdosta. Geological Survey of Finland, archive report M19/2314/-89/2/10. 2 p., 6 app. pages. (in Finnish). Available at: https://tupa.gtk.fi/raportti/arkisto/m19_2314_89_2_10.pdf

Vaarma, M. & Kähkönen, Y. 1994. Geochemistry of the Paleoproterozoic metavolcanic rocks at Evijärvi, Western Finland. In: Nironen, M. & Kähkönen, Y. (eds) Geochemistry of Proterozoic supracrustal rocks in Finland: IGCP Project 179 stratigraphic methods as applied to the Proterozoic record and IGCP Project 217 Proterozoic geochemistry. Geological Survey of Finland, Special Paper 19, 47–60. Available at: https://tupa.gtk.fi/julkaisu/specialpaper/sp_019_pages_047_060.pdf

Vaarma, M. & Pipping, F. 1997. Alajärven ja Evijärven kartta-alueiden kallioperä. Summary: Pre-Quaternary rocks of the Alajärvi and Evijärvi map-sheet areas. Geological Map of Finland 1:100 000, Explanation to the Maps of Pre-Quaternary Rocks, Sheets 2313 and 2314. Geological Survey of Finland. 83 p. Available at: https://tupa.gtk.fi/kartta/kallioperakartta100/kps_2313_2314.pdf

APPENDICES

Appendix 1.

Analyses

Eurofinns Labtium analyses order nr.

Diamond drill hole assays: 40356, 40353, 40358, 40359, 40397A, 40397B, 40397C

Surface sampling: : 47869, 47870

Appendix 2.

Drillhole data

HOLE_ID	Y-koordinaatti	X-koordinaatti	Z-koord	azimuth	dip	length
P4222019R20	7045028.99	325881.77	66.19	100.00	45.00	122.50
P4222019R21	7045059.59	325883.48	65.51	100.00	45.00	128.70
P4222019R22	7044996.28	325880.57	68.38	100.00	45.00	122.90
P4222019R25	7045010.90	325959.42	64.89	280.00	50.00	98.50
P4222019R24	7045130.11	325895.57	64.81	100.00	45.00	146.50
P4222019R23	7045019.15	326019.26	65.16	280.00	45.00	119.40
P4222019R7	7045019.49	325909.97	66.02	99.10	45.50	158.60
P4222019R8	7044789.137	325593.2209	73.6729	96	44.2038	87.5
P4222019R9	7044793.837	325679.3879	73.8715	101.8	45.153	128.35
P4222019R10	7044752.305	325765.0259	69.329	NA	NA	39.8
						tot 1152,75

Appendix 3.

Drill hole cross sections

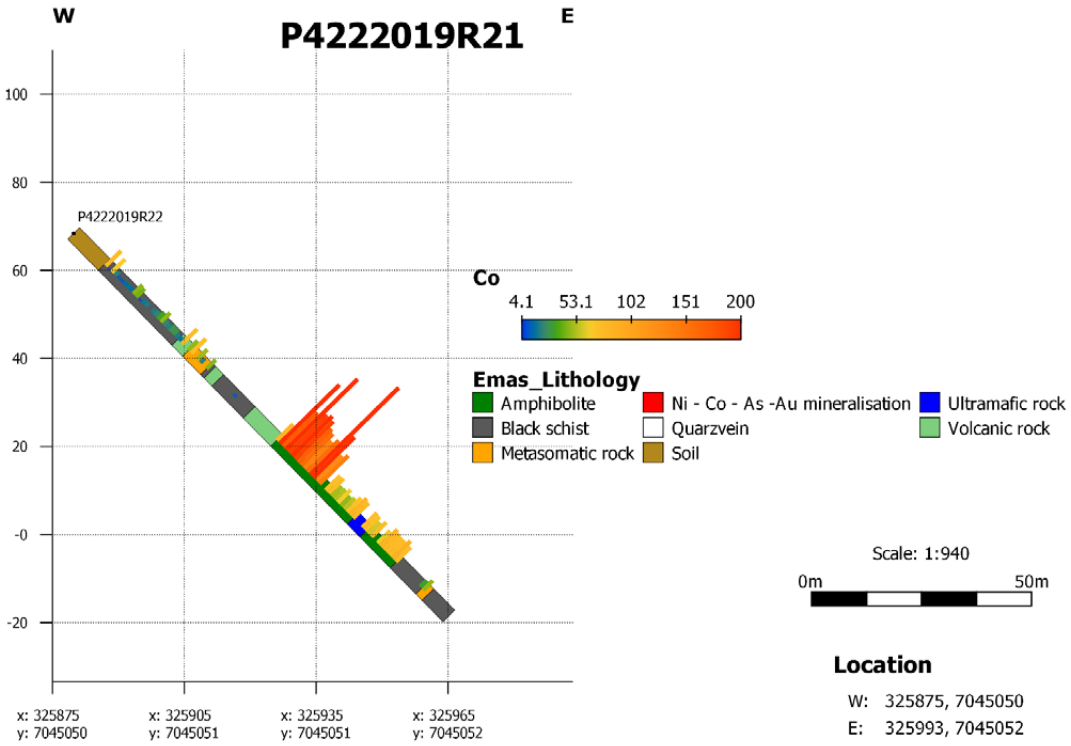

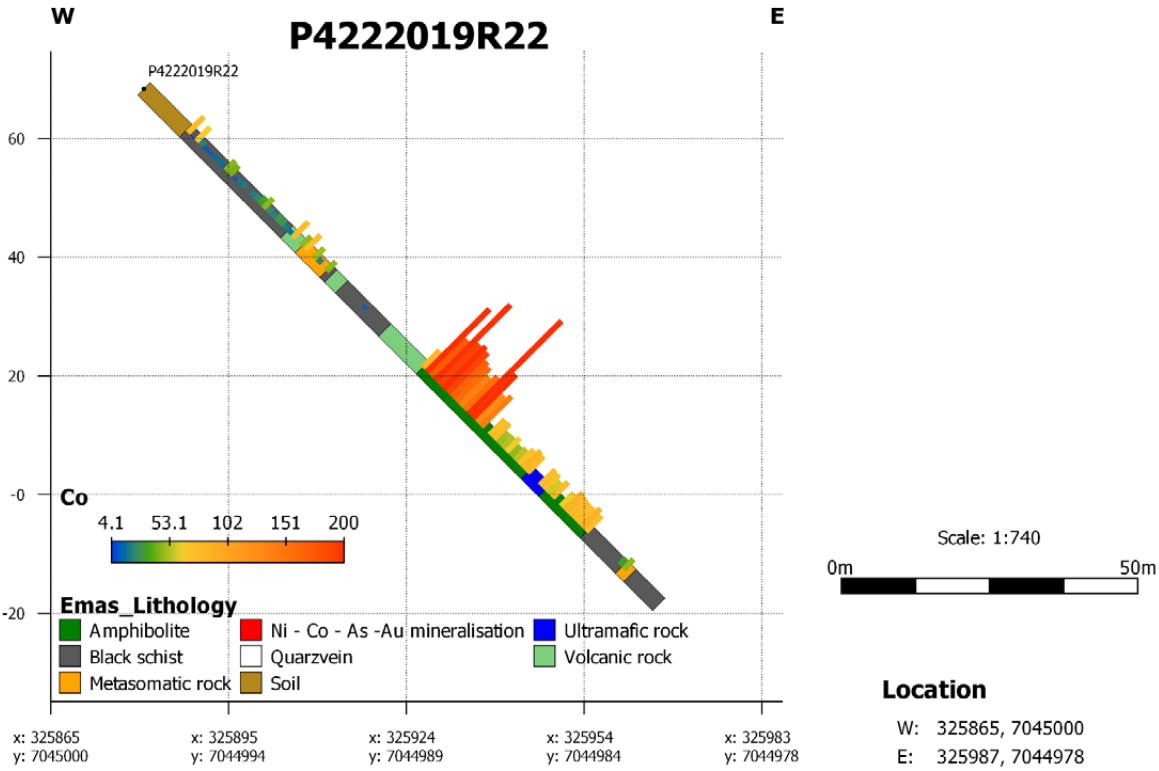

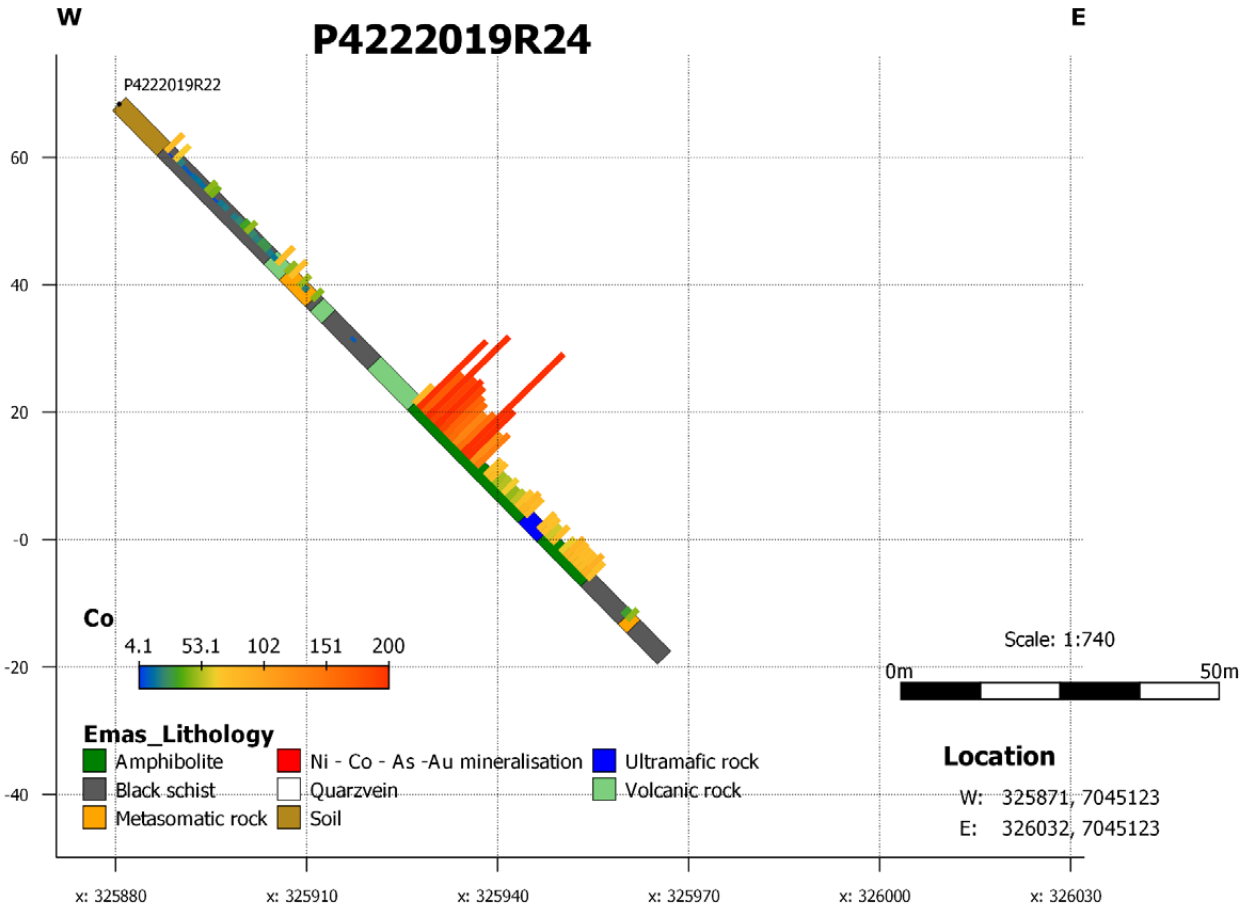
W
E
P4222019R24
P4222019R22
60
40
20
-0
-20
-40
Co
4.1
53.1
102
151
200
Scale: 1:740
0m
50m
Emas_Lithology
Amphibolite
Black schist
Metasomatic rock
Ni - Co - As -Au mineralisation
Quarzvein
Soil
Ultramafic rock
Volcanic rock
Location
W: 325871, 7045123
E: 326032, 7045123
x: 325880
x: 325910
x: 325940
x: 325970
x: 326000
x: 326030

Graphite in drill holes R7, R20 -R25

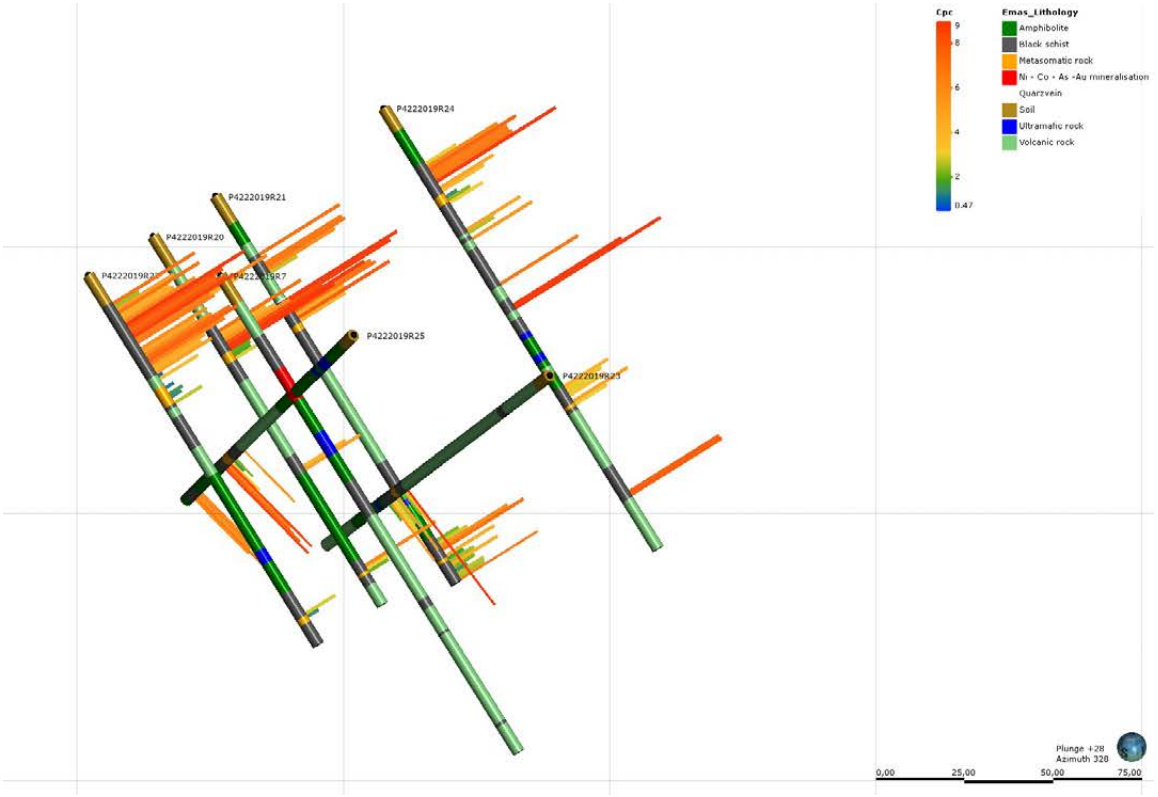

Drill hoes R8 - R10

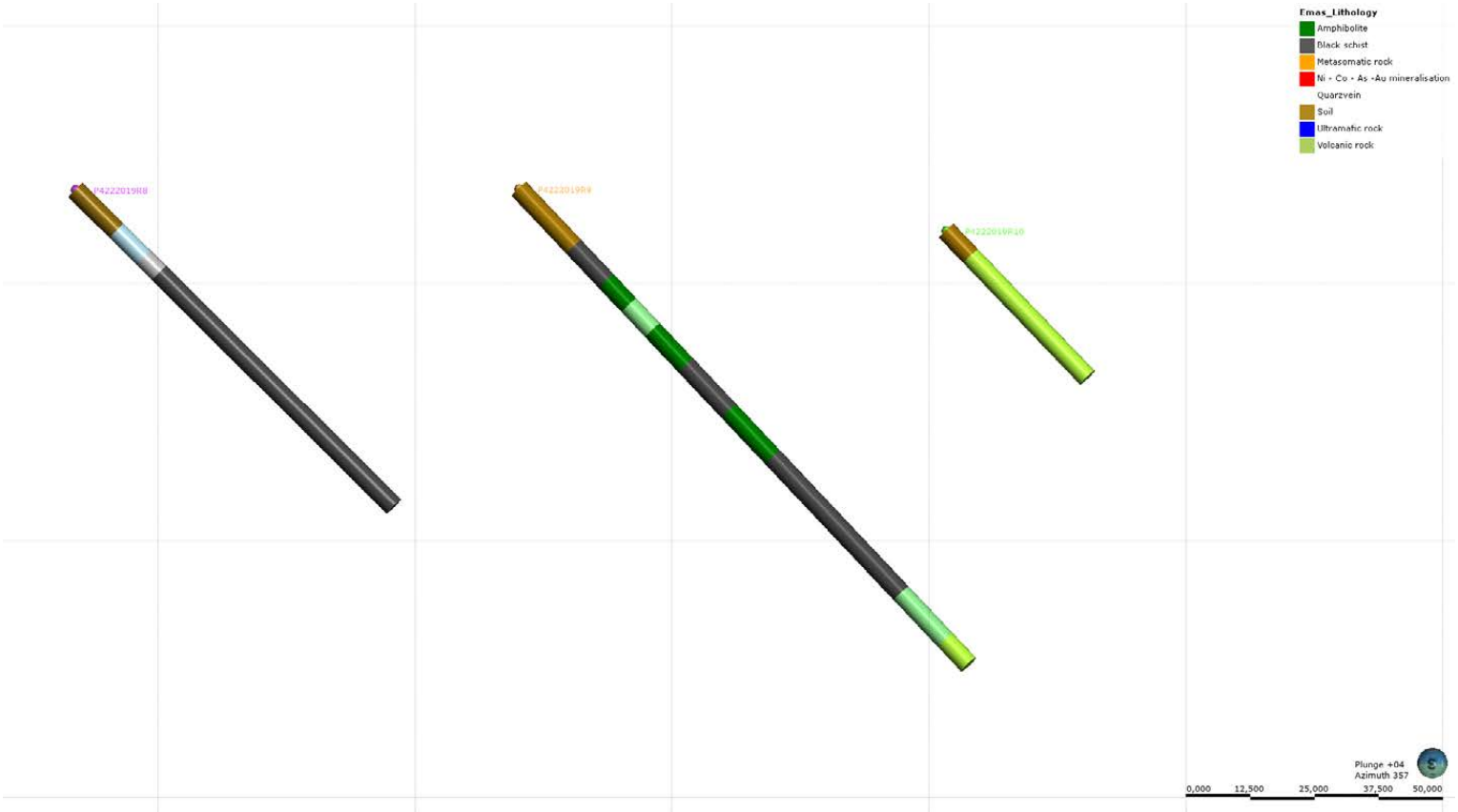

All GTK's publications online at hakku.gtk.fi